An Experimental Comparison of Bubble and Sediment Plumes in Stratified Environments

by

Leah Sarah Reingold

Submitted to the Department of Civil and Environmental Engineering
in partial fulfillment of the requirements for the degree of

Master of Science in Civil and Environmental Engineering

at the

MASSACHUSETTS INSTITUTE OF TECHNOLOGY

September 1994

© Massachusetts Institute of Technology 1994. All rights reserved.

ARCHIVE
MASSACHUSETTS INSTITUTE
OF TECHNOLOGY

OCT 06 1994

LIBRARIES

Author .....
Department of Civil and Environmental Engineering
August 5, 1994

Certified by .....
Dr. E. Eric Adams
Senior Research Engineer
Thesis Supervisor

Accepted by .....
Dr. Joseph M. Sussman
Chairperson, Departmental Committee on Graduate Students

An Experimental Comparison of Bubble and Sediment Plumes in Stratified Environments

by

Leah Sarah Reingold

Submitted to the Department of Civil and Environmental Engineering
on August 5, 1994, in partial fulfillment of the
requirements for the degree of
Master of Science in Civil and Environmental Engineering

Abstract

Environmental applications of bubble plumes require experimental data for bubbles smaller than one millimeter in diameter. It is difficult to obtain a steady flow of bubbles this small in the laboratory, so this study investigates the use of negatively buoyant sediment plumes to model positively buoyant bubble plumes. This procedure benefits from the ease with which sediment is measured, obtained and stored at any desired diameter. In trials comparing sediment and bubbles of the same terminal and slip velocity, in plumes with equal and opposite buoyancy fluxes, sediment is shown to be a good model for air bubbles to determine plume peeling heights in stratified environments. Within margins of experimental repeatability, the bubble plumes and sediment plumes peel at the same distance from their starting points. Further experiments with smaller sediment provide data that is used to generate a graph for determining plume peeling heights; the normalized plume peeling height is found to decrease with increasing sediment size. This normalized curve can applied to bubble plumes by matching slip and terminal velocities. A negatively buoyant liquid plume is observed, and its peeling height is compared both to theoretical single-phase peeling heights and to experimental sediment plume peeling heights. The results for the liquid plume match theoretical estimates for single-phase buoyant plumes, but momentum effects distort the comparison between liquid and sediment plumes. Experimental bubble plume results are compared with previous studies; normalized peeling heights in this work are higher than those in one earlier simulation, but lower than those in another. Bubble plume peeling is observed to cause less diverted volume flux than predicted by a simulation in an earlier work.

Thesis Supervisor: Dr. E. Eric Adams
Title: Senior Research Engineer

Acknowledgments

This work would not have been possible without the constant assistance of colleagues, friends and relatives. Thank you to my advisor Dr. E. Eric Adams, who always made time to answer questions and provide guidance and advice. Special thanks to Mr. Ryan G. Evans of the MIT Media Laboratory, who came to my aid to produce video figures, although I had never met him before. Thank you to my friends in the Parsons Laboratory, who made my working environment a cheery place to be, and to my family for their continued encouragement. Most of all, thank you to my beloved husband Ben, who helped me make figures, photograph results, and stay awake late at night to finish this thesis; his confidence in me was and is one of my greatest sources of strength.

Biographical Note

Leah Sarah Reingold was born on December 29, 1972, in Urbana, Illinois. She is the oldest of four daughters; her parents are Edward and Ruth Reingold. Ms. Reingold attended Yankee Ridge Elementary School and University High School, both in Urbana. In September, 1989, she enrolled at the Massachusetts Institute of Technology (MIT) in Cambridge, MA. She graduated in February, 1993 with her S.B. in Environmental Engineering Science, and continued at MIT as a graduate student in the same field, completing her S.M. in August, 1994.

Ms. Reingold married David Benjamin Gordon (whom she met at MIT) on June 19, 1994. She will therefore be known as Leah Sarah Gordon, with the exception of this work. As of September, 1994, Ms. Reingold will be attending the California Institute of Technology (Caltech) in Pasadena, California, where she will work toward a Ph.D. in Environmental Engineering. Meanwhile, Mr. Gordon will be working toward a Ph.D. in Chemistry, also at Caltech.

Dedication

♡ To Ben, with all my love. ♡

Contents

List of Figures

List of Tables

Chapter 1

Introduction

1.1 Bubble Plume Background

Bubble plumes have many environmental applications. They can be used to aerate lakes and reservoirs [16] [17] [21] [24] [30] [31] [32] [33] [35], prevent ice formation in harbors [3] [2] [4] [34], contain oil spills [1] [13] [25], and prevent salt water intrusion in estuaries [8] [18]. Recently, bubble plumes have been investigated as a means for carbon dioxide sequestration in the ocean [22].

The behavior of bubble plumes in stratified environments has been discussed by many researchers. Scientists have been running bubble plume experiments both in the laboratory and in the field since the 1950's [8] [13] [18] [26]; a few years later, researchers began to investigate bubble plumes in stratified environments [1] [5] [8] [21] [25]. The primary purpose of many such experiments was to investigate bubble plumes for aeration application [16] [17] [31] [32] [35]. Along with laboratory trials, researchers have developed theoretical models for bubble plume behavior [2] [3] [8] [25] [26].

1.2 Sequestration of Carbon Dioxide

1.2.1 Atmospheric Carbon Dioxide

During the hundred and fifty years since the industrial revolution, fossil fuel combustion has increased carbon dioxide (CO_2) levels in the atmosphere. Increased CO_2 levels may cause climate changes, generally referred to as the "Greenhouse Effect" [29]. This effect, which can cause global warming, occurs because CO_2 reradiates infrared radiation back onto the earth's surface [22] [29]. Although opinions vary on how CO_2 will affect the atmosphere, it is clear that the increases in atmospheric CO_2 are significant compared to the low ambient levels. (The atmosphere currently contains an estimated 300 *ppmv* of CO_2 [15] [29].) Although a decrease in the use of fossil fuels would reduce CO_2 output to the atmosphere, this option is not feasible without large changes in worldwide lifestyle; that alternative is therefore not realistic. This is especially true for developing countries, in which large reductions in energy consumption would be disastrous for local economies.

At the current rate of fossil fuel consumption, levels of atmospheric CO_2 are projected to rise as fossil fuel resources become depleted to the point at which they are no longer a viable economic alternative. At that point, the ocean will take up the excess CO_2 from the atmosphere. Currently, the ocean contains about 0.1 $\frac{kg}{m^3}$ CO_2; at saturation, however, it has the potential to dissolve 40 to 50 $\frac{kg}{m^3}$ [22]. If this equilibration occurs naturally, CO_2 levels will peak in the next few hundred years, before decreasing through ocean absorption. To avoid the surge of atmospheric CO_2, researchers have considered forcing the ocean to take up excess CO_2 directly, as soon as it is produced by power plants. The CO_2 would be isolated from flue gas, and then piped deep into the ocean, to be released as bubble or droplet plumes [22].

1.2.2 Carbon Dioxide Bubble Plume Models

Underwater plumes are formed when CO_2 is released into the ocean in various phases. The phase of the CO_2 is determined by release depth. At less than around 500 m below

the ocean surface, CO_2 is in the vapor phase. It can be released as bubbles or as liquid that flashes into vapor upon release. Between around 500 m and around 3000 m below the surface (depending on temperature), CO_2 is released as positively buoyant liquid droplets. Below around 3000 m, CO_2 is a negatively buoyant liquid [22]. Practical considerations discourage transport of CO_2 much below 1000 m, however, so only positively buoyant plumes are discussed in this work.

After being released, CO_2 bubbles create a plume that entrains sea water as it rises through the ocean; the entrained water dissolves the CO_2 bubbles as they moves upward. The bubbles form a plume, which evolves as follows: Because the ocean is density-stratified, the rising plume carries with it water that is denser than the local ambient fluid. This causes the plume (a mixture of bubbles and entrained water) to become less buoyant as it rises. When the upward buoyancy force due to the bubbles is sufficiently counteracted by the downward buoyancy force of the entrained dense water, the outer annulus of the plume "peels" off and intrudes into the ambient sea water. After the plume has peeled, the remaining bubbles continue to rise, creating a new plume. Although experimental observations have been limited to single peeling events [25], the peeling and restarting process can be expected to continue as long as there are bubbles in the plume to provide upward momentum, as shown in figure 1-1. The peeled water contains dissolved CO_2; each peel leads to a reduction of CO_2 in the plume and an increase in ambient dissolved CO_2. Eventually, shortly after all of the CO_2 has been dissolved, the plume has no more upward momentum; at this point, the plume peels to the sides, and is considered to have reached its "trap height."

Carbon dioxide released as an underwater plume will stay in the ocean only if the bubbles are released deeply enough in the ocean for all of the CO_2 to dissolve into the water and be carried away by peeling. Plumes must be released deeply enough below the ocean surface to ensure that they reach trap height below the ocean's well-mixed layer, which begins at around 100 m below the ocean surface. If dissolved CO_2 enters the well-mixed layer, it can then be released back into the atmosphere very quickly. Even if the plume is trapped below the well-mixed layer, some CO_2 will eventually escape back into the atmosphere. The CO_2 residence time in the ocean, however,

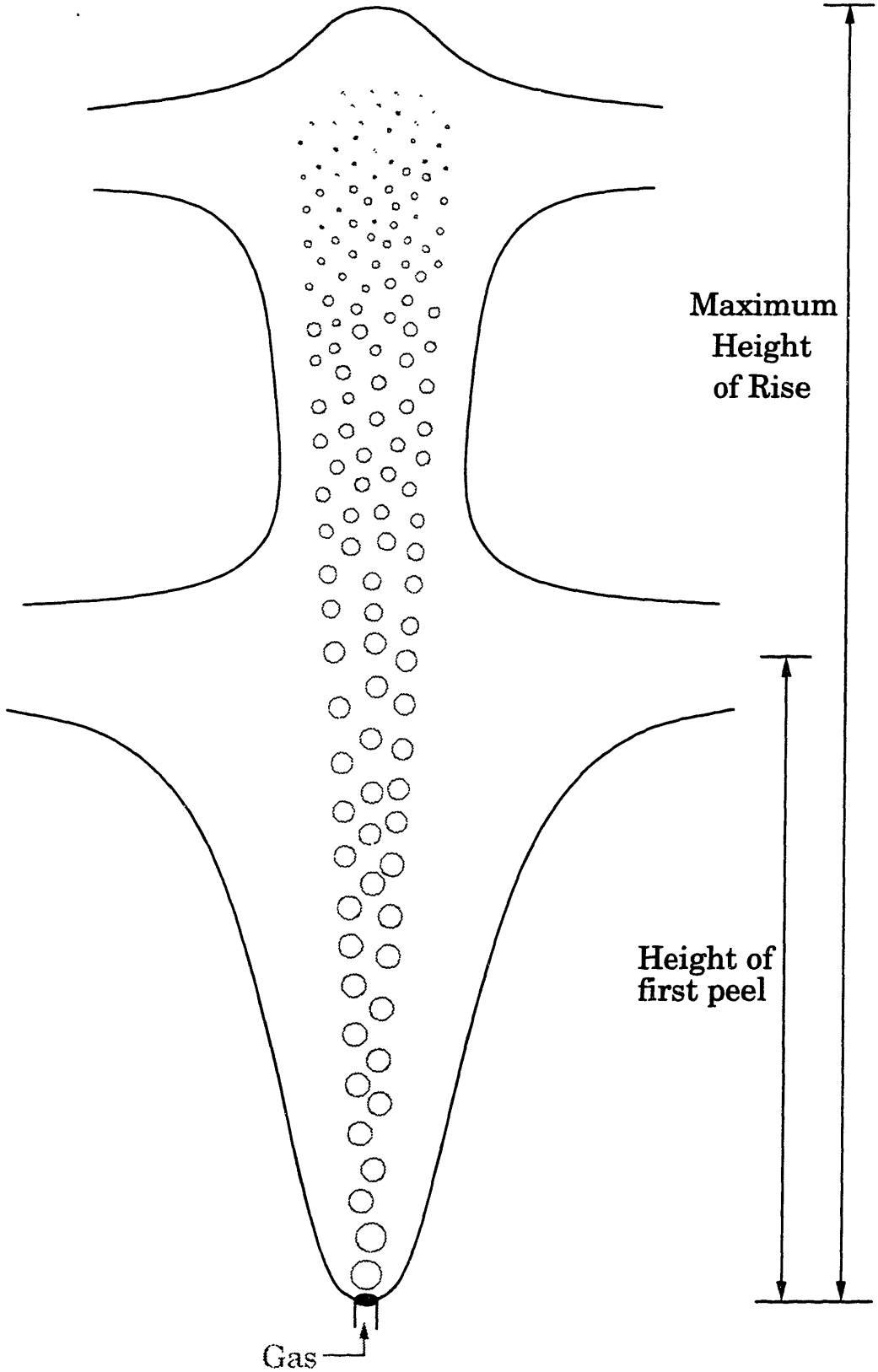

Figure 1-1: Schematic of Bubble Plume Peeling and Restarting Process

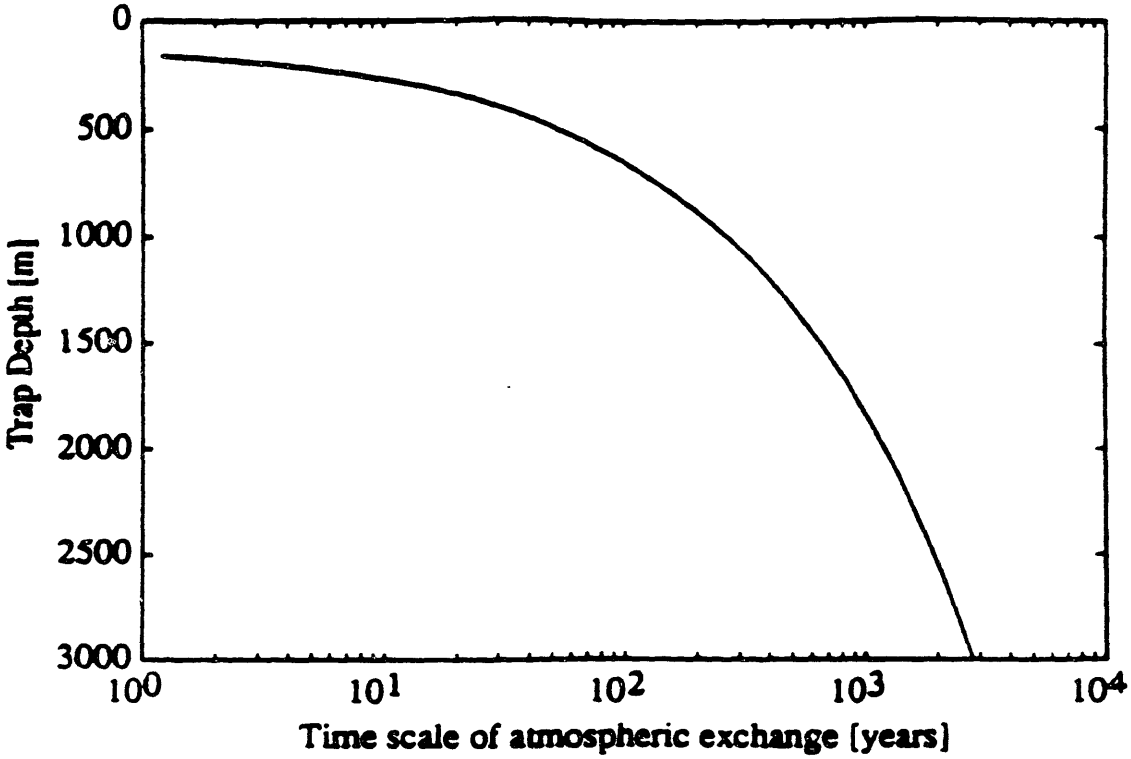

Figure 1-2: Residence Time of Carbon Dioxide vs. Release Depth; Liro, 1991

is greatly increased if the plume is trapped below the well-mixed layer, as shown in figure 1-2 [22].

In 1991. Christopher R. Liro modeled CO_2 plumes in the ocean using a Runge-Kutta simulation model. The Liro model was a dual study of fluid plume motion and CO_2 bubble dynamics. The plume was modeled with an integral jet analysis, based on equations of conservation of mass, conservation of momentum and conservation of buoyancy. Bubbles were analyzed by equations of gas transfer and bubble rise velocity. The Liro model made several simplifying assumptions relevant to this work: Plume properties (velocity and gas concentration) were assumed to be described by self-similar Gaussian profiles. Also, peeling was assumed to take place when the net upward buoyancy force was equal to the net downward buoyancy force. In addition, one half of the plume volume was assumed to peel off in each peeling event.

His results showed that plume trap height could be made to occur at a greater depth in the ocean by varying three plume parameters: the plume could be released

deeper in the ocean, the plume could be released as several parallel plumes by means of a multi-port diffuser, or the initial bubble radius could be reduced. Deeper release and more outlets are both expensive options that increase the amount of space required for the CO_2 nozzle. Given an extant multi-port set-up, it is therefore useful to investigate options for reducing trap height without changing the location of the release. Smaller initial bubble diameter is such an option. For this work, the Liro model was modified to record intermediate data during simulations. Also, additional computer procedures were developed for calculating average ambient CO_2 concentration and pH from the data for each experiment. The model was then run with bubbles of smaller initial radius; the results appear in figures 1-3, 1-4, 1-5, and 1-6. For these runs, the model parameters were kept constant as in the Liro base scenario [22], with an assumed CO_2 loading of 133 $\frac{kg}{s}$ (as would be expected from a typical power plant). The data shown in these figures is for a one-port system. Calculations of ambient pH were based on predicted concentrations of dissolved CO_2 and their effect on the carbonate-bicarbonate cycle.

As shown in figure 1-3, smaller bubbles lead to earlier plume peeling. However, the earlier peeling and lower eventual trap height cause all of the CO_2 to be dissolved over a smaller distance, leading to higher concentrations of dissolved CO_2 immediately around the plume, as shown in figure 1-5. These higher concentrations lead to greater shifts in the carbonate-bicarbonate cycle of the ocean, and cause substantial downward pH shifts immediately surrounding the plume, as depicted in figure 1-4. The pH calculations were based on a weighted average of the CO_2 concentrations in the layers of peeled plume fluid, shown in figure 1-5; ambient ocean pH is usually around 8.

According to the Liro model, bubbles sized on the order of 1 mm in diameter would create a plume with trap height one tenth as high as that of a plume of 1 cm diameter bubbles. Bubbles smaller than 1 mm in diameter reduce trap height even more, as shown in figure 1-6. The Liro model cannot be extended indefinitely, however, so more research is needed to focus on smaller bubbles.

It is necessary to determine how these smaller bubbles behave in bubble plumes;

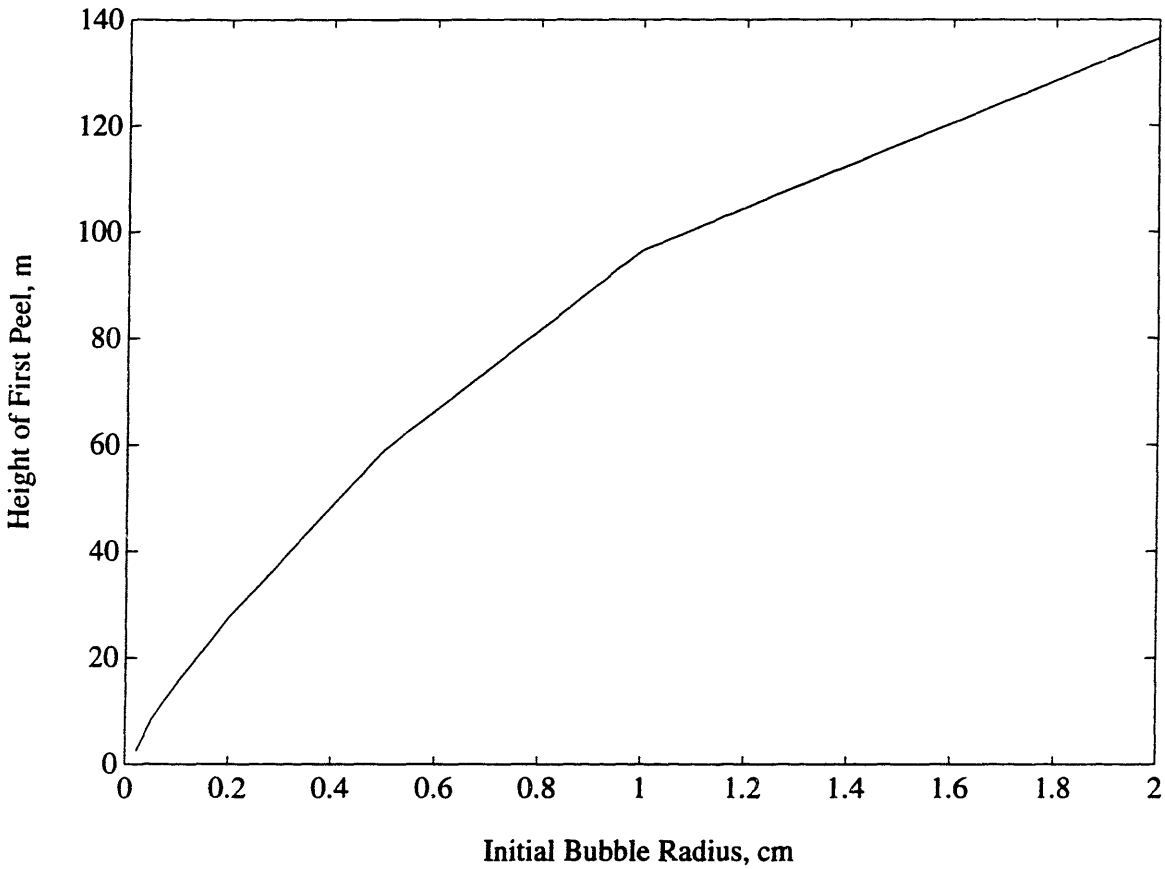

Figure 1-3: Height of First Peel vs. Initial Bubble Radius, Liro Base Scenario

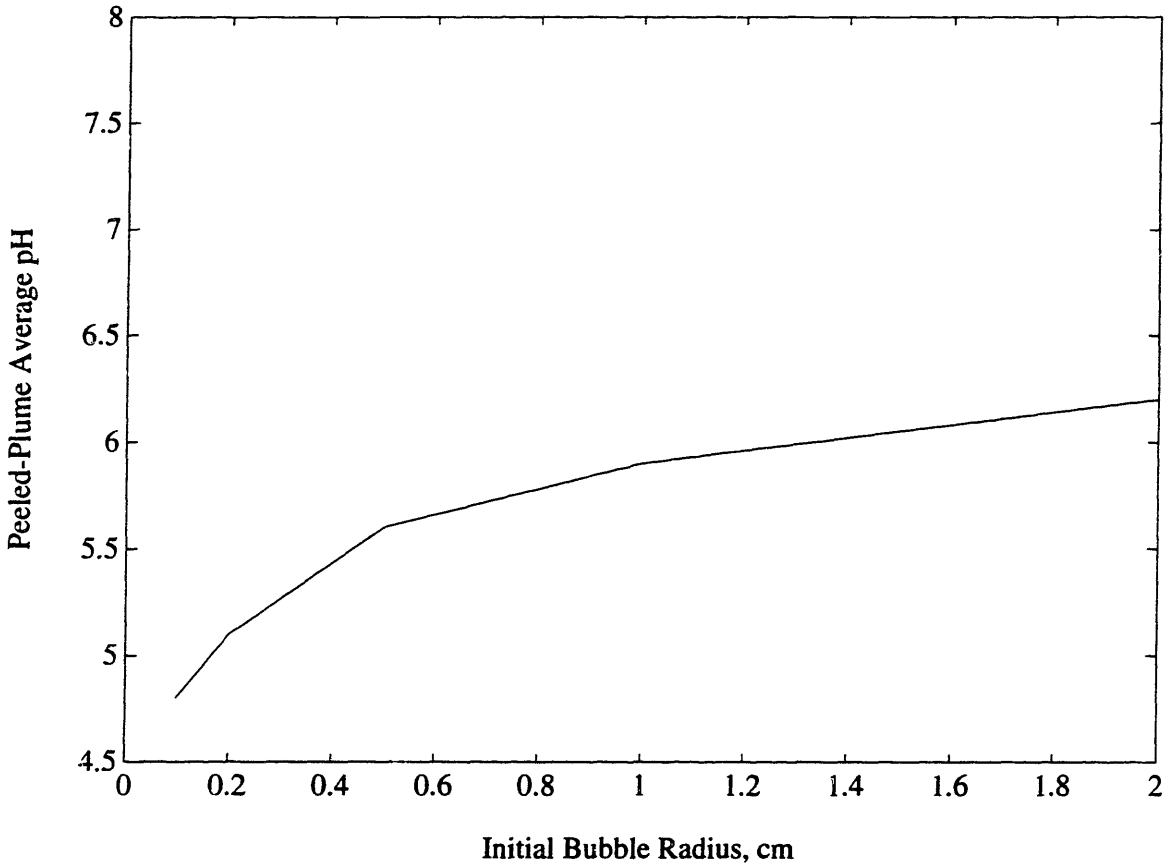

Figure 1-4: Local pH vs. Initial Bubble Radius, Liro Base Scenario

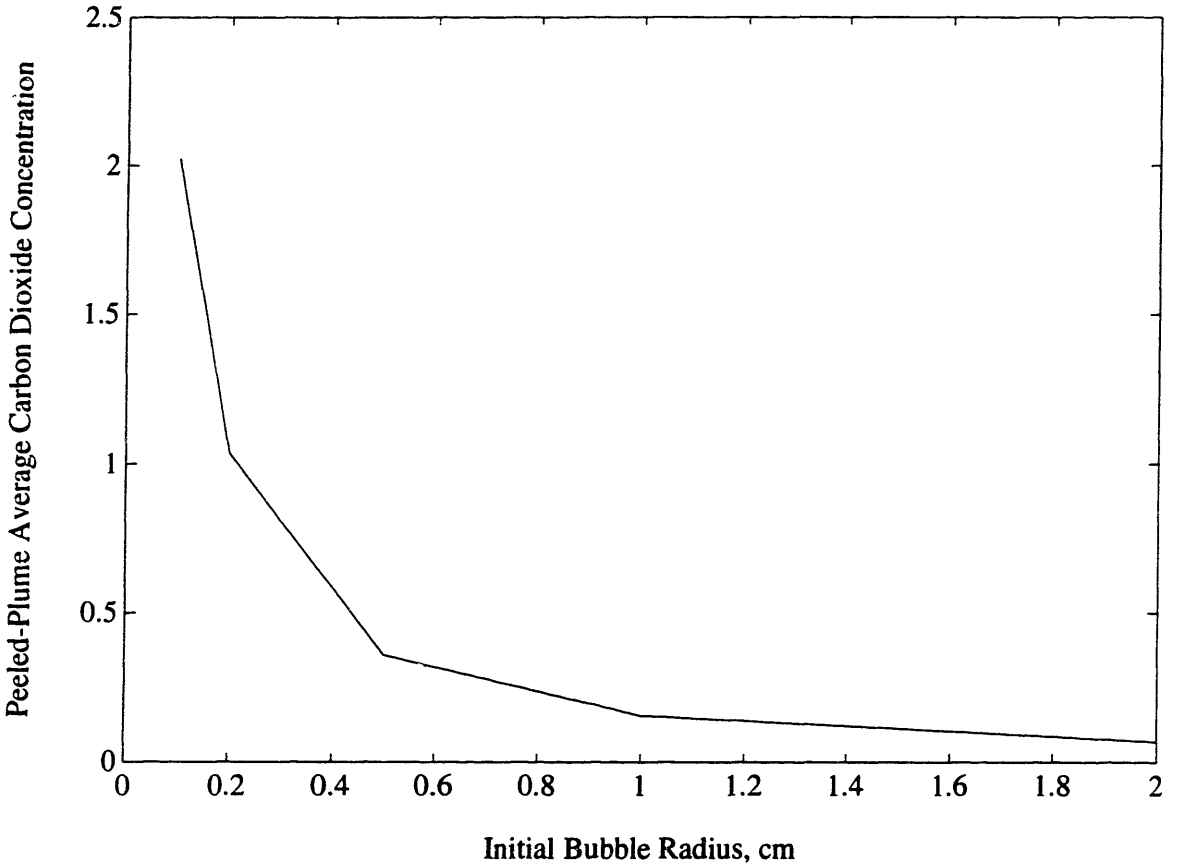

Figure 1-5: Local CO_2 Concentration vs. Initial Bubble Radius, Liro Base Scenario

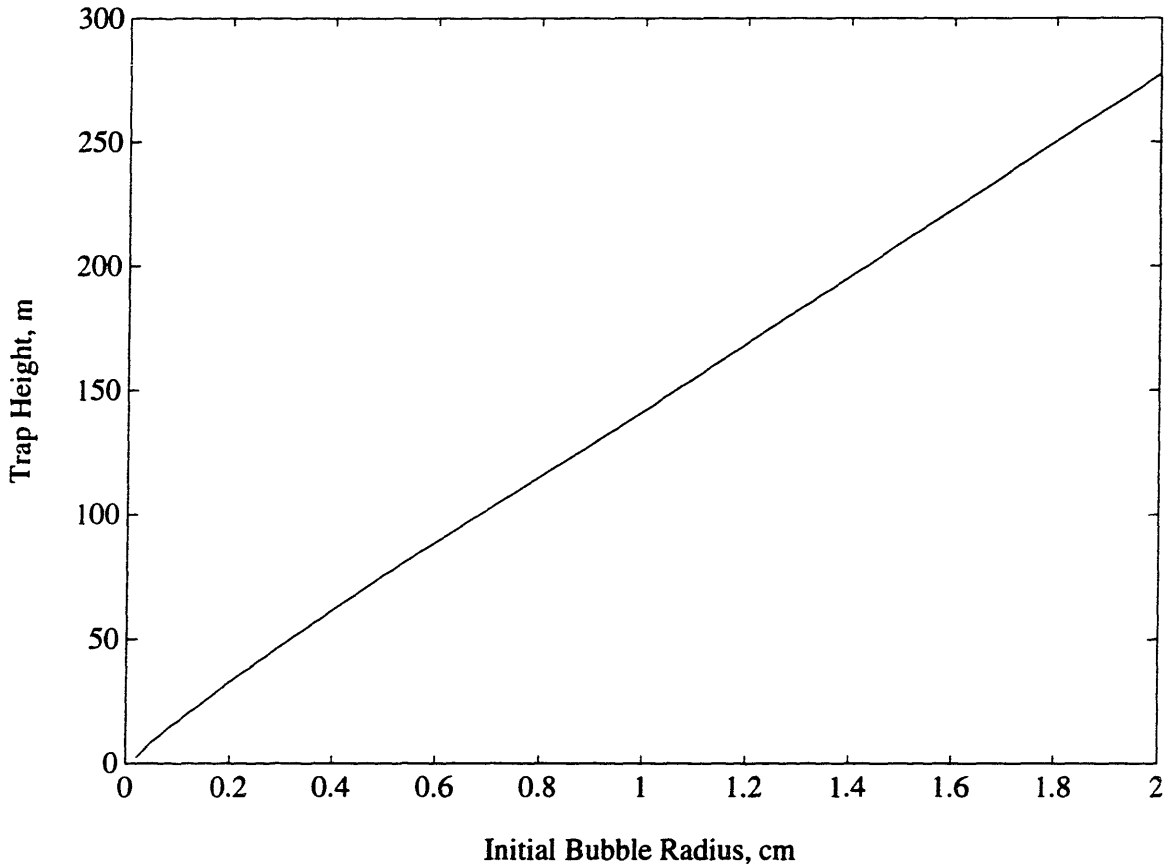

Figure 1-6: Trap Height vs. Initial Bubble Radius, Liro Base Scenario

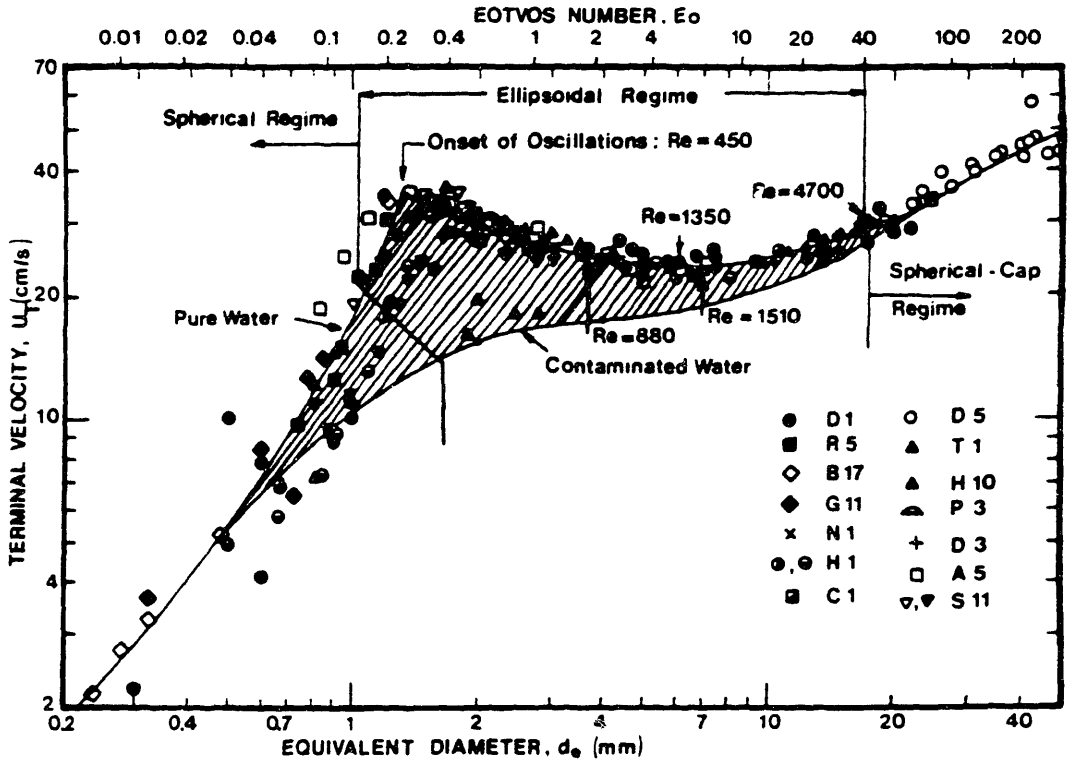

Figure 1-7: Bubble Shape and Slip Velocity vs. Equivalent Diameter: Clift, 1978

many models, including Liro's, rely on assumptions of elliptical shape and internal fluid motion that are true only for bubbles larger than 1 *mm* in equivalent diameter. Figure 1-7 [9] shows how bubble slip velocity and shape vary with equivalent bubble diameter. A drawback to further research on very small bubbles, though, is that a continuous stream of such bubbles (smaller than 1 *mm* in diameter) is difficult to generate repeatably in the laboratory, so bubble plume studies have thus far focused on larger bubbles, rather than on plume dynamics for smaller bubbles. Liro, for example, focussed on larger bubbles to be conservative: If the larger bubbles (or droplets) could dissolve below the well-mixed zone in the ocean, then so could smaller bubbles [22]. The difficulties associated with very small bubbles are discussed further in section 2.1.

In the limit of infinitessimally tiny bubbles, a bubble plume is expected to be similar to a plume of a positively buoyant liquid, with an evenly distributed buoyancy source. Calculations for this case provide a theoretical limit on parameters affected by bubble size; this is discussed further in section 2.3.1.

Chapter 2

Motivation and Theory

2.1 Small Bubbles

Gas bubbles are usually produced by the break-up of a turbulent gas jet. This method tends to produce bubbles that are stable at diameters between around 2 *mm* [6] and around 5 *cm* [9]. If the bubbles are released at larger sizes, they break up; if they are released at smaller sizes, they coalesce [5] [6] [25]. As discussed in section 1.2.2, plumes of small gas bubbles may have useful environmental applications. Bubbles smaller than 1 *mm* in diameter, however, are difficult to generate in a controlled, repeatable fashion in the laboratory.

In order to produce smaller bubbles, the turbulent gas jet break-up method must be replaced by other experimental techniques such as atomization, during which excess energy is introduced to the system [9]. This excess energy interferes with ideal pure plume behavior, complicating plume observations. In the field, where bubble plumes are used over much greater depths, this near field effect would have less influence on later plume behavior, so environmental applications of small bubbles may well be possible. In order to study bubble size for application, however, preliminary laboratory trials are necessary.

There is motivation, then, for studying very small bubbles and their behavior in bubble plumes, but it is difficult to produce repeatable small bubble plume data. This work undertakes to use small sediment to model small bubbles, to derive con-

clusions about their behavior in plumes. Sediment may provide a useful model for bubble behavior, as discussed in the following sections. If sediment is shown to be an accurate model for bubbles, then there are several directions for experimentation. For example, dissolving sediment could be used to model dissolving-gas bubbles, or flocculant sediment could be used to model coagulating bubbles. Furthermore, the sediment plume data can be applied directly to other environmental applications, such as the problem of a continuous marine release of CO_2 hydrates.

2.2 Comparison of Bubbles to Sediment

Non-cohesive sediment is well-suited to model bubbles in plumes, because both sediment and air can be made to enter water in steady streams of particles. Furthermore, there is reason to believe that a downward plume of sediment grains is similar to an upward plume of bubbles, because the relative densities of the two media compared to water are approximately equal in magnitude (though opposite in sign). The sediment used has a density of 2.6 $\frac{g}{cm^3}$ (as measured in preliminary experiments); the density of water is approximately 1.0 $\frac{g}{cm^3}$ even when it contains some salt. Air has density close to zero relative to water or sediment. Therefore, the relative density to water of the sediment used is 1.6 $\frac{g}{cm^3}$, while the relative density to water of air is -1.0 $\frac{g}{cm^3}$. These values are the same size within a factor of two; to compensate for the difference, the buoyancy fluxes can be kept equal by adjusting flow rates as described in section 3.2.

Sediment differs from bubbles in several useful ways, all of which result from the lack of surface tension phenomena in sediment particles. Non-cohesive sediments, unlike small bubbles, do not coalesce; large gravel pieces, unlike large bubbles, do not break up spontaneously. Moreover, sediment is easily sifted into different sizes, ranging from dust to boulders. Finally, small sediment can be introduced to water without any excess energy production, unlike small bubbles, which must be atomized by highly energetic processes, as discussed in section 2.1.

Therefore, if useful parallels are discovered between the behavior of sediment plumes and that of bubble plumes, then small sediment can be used to model small

bubbles, and bubble size can be optimized (by means of sediment trials) for environmental application. Sediment trials would be repeatable, because of the ease of obtaining and using small sediment. With the knowledge of optimal sediment (and hence bubble) size, bubbles could be generated at the right size for final application, without the attendant preliminary experimentation.

Some varieties of sediment plumes are useful in the environment. For example, instantaneous releases of dredged material have been studied [19] [23] [28], as has been sediment transport in river beds [12] [20]. Steady sediment plumes in vertical free fall, however, have few useful applications in the environment, and are therefore notably absent in the literature. They differ from dredged disposal because they are continuous, and they differ from sediment transport because they are vertical, with negligible effects from coasts or bottom. This work undertakes to study steady sediment plumes in vertical free fall, hopefully to develop useful comparisons with bubble plumes.

2.3 Theoretical Plume Buoyancy Distribution

2.3.1 Background Discussion

Bubble and sediment plumes behave differently than plumes of a single-phase buoyant fluid. Bubbles and sediment are contained mostly in the central core of the plume [22] [25]. A fresh-water plume in salt-water, by contrast, has more evenly distributed buoyancy.

Previous experiments have investigated the quantitative relationship between bubble diameter and bubble distribution in a plume [8] [22]. The larger the bubbles or sediment, the more confined they are to the central core of the plume. Smaller bubbles or sediment can spread more evenly throughout the plume, aligning themselves more closely with the Gaussian distribution of plume velocity. In the limit, then, of very small bubbles or sediment, the plumes would behave as though they were plumes of buoyant liquid. Calculations are shown in section 2.3.2 to determine the theoreti-

cal maximum height of rise of this limiting case (h_{max}), and the other characteristic plume heights associated with h_{max}.

Because the bubbles in a two-phase plume are large enough to be confined to an inner core of the plume, their applied buoyancy force can act only on the fluid adjacent to the inner core of the plume. This limited range of buoyancy influence affects the plume dynamics; the entrained fluid is under less forcing than if the plume were evenly buoyant, and peeling can occur closer to the plume source. The theoretical limiting plume height, therefore, is expected to be longer than the experimental height of first peeling in a two-phase plume. Although the following discussion describes bubble plumes, the phenomenon applies equally to sediment plumes.

2.3.2 Determination of Characteristic Plume Heights

There are three characteristic plume heights; two can be be determined from plume theory. These are the maximum height of rise (h_{max}) and the height of neutral buoyancy (h_{neut}). The third characteristic plume height (the experimentally observed peeling height) is predicted to fall between h_{max} and h_{neut}. Figure 2-1 shows the qualitative relationship between the height of neutral buoyancy, the peeling (or trap) height and the maximum height of rise for a given single-phase plume. The behavior of a single-phase buoyant plume depends on two basic parameters. The first parameter is the kinematic buoyancy flux:

$$B_0 = g\frac{\Delta\rho}{\rho}Q_0, \tag{2.1}$$

where g is gravitational acceleration, $\frac{\Delta\rho}{\rho}$ is the density difference between the bubbles (or sediment) and the ambient fluid (normalized by the fluid density), and Q_0 is the volume flow rate of the air (or sediment). The second parameter is the square of an equivalent stratification frequency:

$$\varepsilon = |\frac{g}{\rho}\frac{d\rho}{dz}|, \tag{2.2}$$

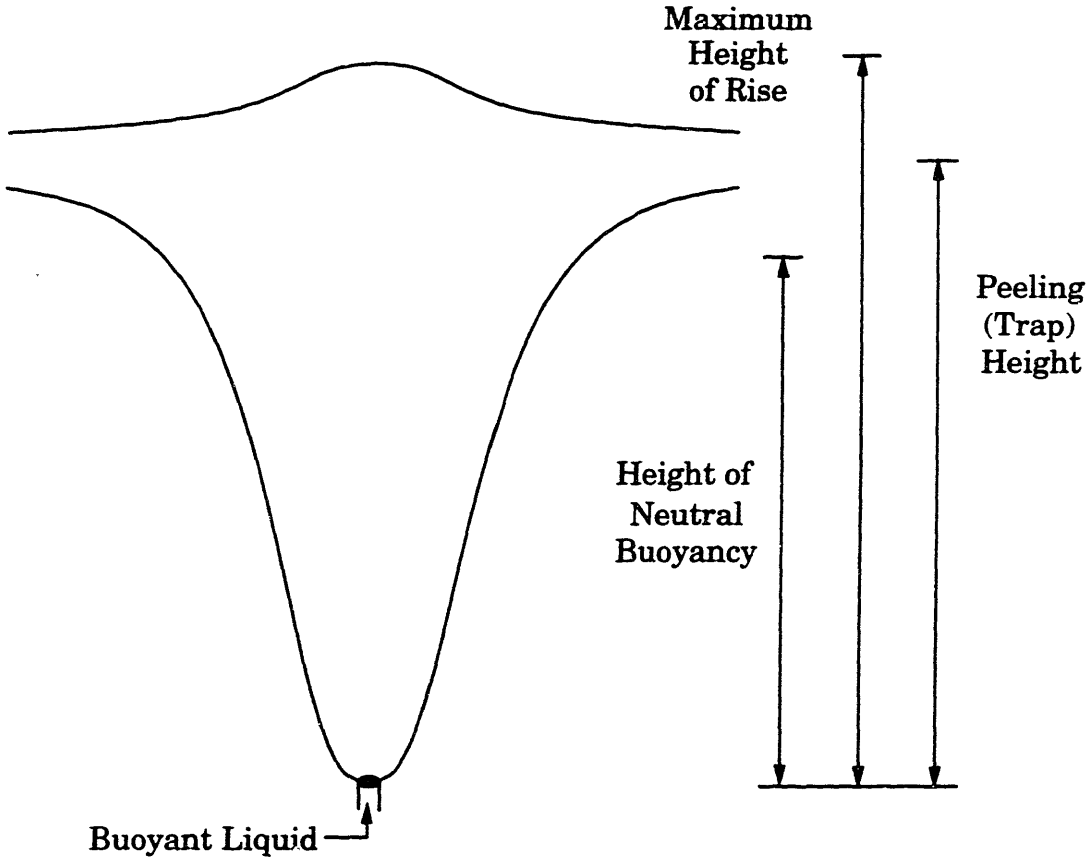

Figure 2-1: Qualitative Picture of Trapped Single-Phase Plume

where ρ is the ambient fluid density and $\frac{d\rho}{dz}$ is the vertical ambient density gradient. From dimensional analysis, the maximum height of rise should be proportional to $\frac{B_0^{\frac{1}{4}}}{\varepsilon^{\frac{3}{8}}}$, and experimental results suggest that [7] [14]:

$$h_{max} = 3.8\frac{B_0^{\frac{1}{4}}}{\varepsilon^{\frac{3}{8}}}. \tag{2.3}$$

For example, in the base case experimental bubble plumes discussed in section 4.1, the variables would be:

$$Q_0 = 3.6\frac{cm^3}{s} \tag{2.4}$$

$$\frac{\Delta\rho}{\rho} = 1 \tag{2.5}$$

$$g = 981\frac{cm}{s^2} \tag{2.6}$$

$$\rho = 1\frac{g}{cm^3} \tag{2.7}$$

$$\frac{d\rho}{dz} = \frac{0.0135\frac{g}{cm^3}}{57.4cm} \tag{2.8}$$

leading to a reference maximum height of rise:

$$h_{max} = 51cm. \tag{2.9}$$

For the corresponding base case experimental sediment plume, the flow rate (Q_0) and the density difference ($\frac{\Delta\rho}{\rho}$) are different than those used in the previous calculation:

$$Q_0 = 2.25\frac{cm^3}{s} \tag{2.10}$$

and

$$\frac{\Delta\rho}{\rho} = 1.6 \text{ (but negatively buoyant)}. \tag{2.11}$$

These parameters, however, were selected so that they would result in the same

buoyancy flux, and therefore, under the same stratification, the theoretical maximum height of rise (or depth of sinking) would again be:

$$h_{max} = 51cm, \tag{2.12}$$

measured down from the top of the water surface.

The height of neutral buoyancy (h_{neut}) for a single-phase plume is defined as the distance from the plume source to the elevation at which the positive and negative buoyancies are equal. It is less than the theoretical maximum height of rise, because the plume is carried beyond the height of neutral buoyancy by its momentum. Peeling occurs above h_{neut}, though, because the plume becomes slightly diluted with the lighter, higher ambient fluid, and then settles back down to its peeling height, somewhat above the previous height of neutral buoyancy. The quantities h_{neut} and h_{ref} can be related theoretically [11]; h_{neut} has been found to be between $0.71h_{max}$ and $0.76h_{max}$. These values translate into a factor multiplying $\frac{B_0^{\frac{1}{4}}}{\varepsilon^{\frac{3}{8}}}$ of between 2.7 and 2.9. Furthermore, if plume entrainment in a stratified environment is similar to entrainment in unstratified water, following a $\frac{5}{3}$ power relationship with elevation, then h_{neut} is calculated to be $2.9\frac{B_0^{\frac{1}{4}}}{\varepsilon^{\frac{3}{8}}}$ [27].

For the plume examples above, h_{neut} would therefore be expected to be between about 36 *cm* and about 39 *cm*, assuming behavior similar to that in a single-phase plume. Under this assumption, trapping (peeling) would be expected at some height between 36 *cm* and 51 *cm* beyond the plume source, because when the plume is trapped, it peels away to the sides, just below the maximum height of rise, and above the height of neutral buoyancy.

Chapter 3

Experiment

3.1 Approach

There were two sets of experiments in this work. First, parallel plumes were created of bubbles and sediment. The plume experimental parameters were set from basic assumptions, to create bubble and sediment plumes that were most likely to behave similarly to each other. The results from these experiments were then analyzed, in the hope of developing useful comparisons between bubble and sediment plume behavior. Second, experiments were performed on sediment plumes using smaller grain sizes, to gain further understanding and predictions for plumes of small bubbles.

3.2 Parameters

Experiments were performed to determine parallels between bubble and sediment plumes. Parameters for these trials were selected that were thought most likely to lead to similar plume performance. Although the theoretical motivation for this work is based on carbon dioxide plumes, the experiments presented here were performed using air. Gas transfer and bubble expansion are different for the two gases, but the plume dynamics are expected to be the same, based on the same gas density (negligible relative to water) and bubble size. For the first part of this work, sediment and bubble plumes were created to be as similar to each other as possible.

Sediment Size Range	*Average Measured Terminal Velocity* (v_t), $\frac{cm}{s}$
$0.088 - 0.125mm$	1.5
$0.18 - 0.21mm$	2.1
$0.71 - 0.84mm$	9.7
$1.41 - 2.83mm$	19
$2.83 - 4.00mm$	22
$4.00 - 5.66mm$	27
$5.66 - 6.35mm$	32

Table 3.1: Sediment Terminal Velocity

For these plumes, sediment sizes were chosen based on experimentally determined terminal velocity data, so that their terminal velocity would match the slip velocity of the experimentally obtained air bubbles. For the bubbles, which were on average 0.7 *cm* in equivalent diameter (as determined by visual observation), a slip velocity of 19 $\frac{cm}{s}$ was determined [9] from figure 1-7. To ensure an equal terminal velocity, sediment was chosen in the range of 1.41 *mm* to 2.83 *mm* in sieve-measured equivalent diameter, based on preliminary settling velocity trials. The sediment was sifted and sorted by diameter into several size intervals. Samples from each size range were then dropped into a graduated cylinder (41 *cm* tall, with a 6.5 *cm* internal diameter), and were timed falling past a measured distance after achieving terminal velocity. Terminal velocity was calculated by dividing the known path length by the travel time. The average measured velocity (v_t) for each sediment size range is shown in table 3.1.

Positive and negative buoyancy fluxes were then set equal and opposite to one another. As discussed in section 2.3.2, the kinematic buoyancy flux is $B_0 = g\frac{\Delta\rho}{\rho}Q_0$. For sediment, Q_0 was defined to be the mass flow rate ($\dot{m}$) divided by sediment density. Because the buoyancy flux depends on normalized density difference ($\frac{\Delta\rho}{\rho}$) and flow rate (Q_0), flow rates were adjusted to compensate for the slightly imbalanced density differences. (As discussed in section 2.2, the sediment used has a relative density to water of 1.6 $\frac{g}{cm^3}$, while that of air is -1.0 $\frac{g}{cm^3}$.) Therefore, while the sediment had a mass flow rate of 5.8 $\frac{g}{s}$ ($= 2.23$ $\frac{mL}{s}$), a slightly higher air flow rate was selected (3.6 $\frac{mL}{s}$).

3.3 Equipment

Experiments were performed in a metal tank, which was 1.38 m wide by 3.06 m long by 0.80 m deep. A glass side-wall enabled observations. To improve visibility, a brightly colored sheet metal dividing wall was placed parallel to the glass wall in the tank, between the glass wall and the back wall (42 cm away from the glass wall). Observations were obtained visually and photographically, assisted by a mounted tape measure, stop watch and video camera.

A density-stratified environment was established in the tank before each experiment; salt was the stratifying agent. Salt-water layers were mixed in an elevated basin before being siphoned to the tank. To minimize vertical mixing while the tank was filled, the salt-water layers were poured onto a square plastic splash plate (25 cm to a side), held afloat by adjustable polystyrene foam floats. The splash plate was held in place laterally by a corner of the tank and a suspended metal bar.

Bubble plumes were created by a round vertical air jet at a height of 8.5 cm above the bottom of the tank; the orifice diameter was 0.2 cm. Air was supplied from a compressor via copper tubing, and the air flow rate was regulated by a pressure gage mounted on the side of the tank. The pressure gage was fitted with a "hold" switch to allow maintenance of a given air pressure. Each sediment plume consisted of a steady stream of small stones. The sediment was introduced into the tank from a plastic jug with an orifice at the water surface, and the sediment flow rate was regulated by the size of the entry orifice. Sediment grain size was controlled by pre-sifting sediment into a range of equivalent diameter intervals. Dye was applied with every plume as a passive tracer. Schematic diagrams of the apparatus, as well as a more complete discussion of the procedures, are located in section 3.4.

3.4 Procedures

3.4.1 Stratification

In preparation for plume experiments, the tank was linearly stratified by density; table salt ($NaCl$) was the stratifying agent. Stratification was accomplished by the consecutive introduction of ten distinct layers of salt-water, in order of decreasing salinity, (from 30 *ppt* on the bottom of the tank, to 3 *ppt* at the surface). Each layer was mixed in an elevated vat, and then siphoned onto a splash plate confined in the tank as described in section 3.3. The layers were allowed to stand and diffuse for 36 to 48 hours, leading to an approximately linear profile, as described in appendix A. Salinities were measured with a calibrated salinity probe, and densities were determined from published tables [10].

3.4.2 Air

Air bubble plumes were created by an air jet into the tank. Air flowed into the tank from a vertical air nozzle at the base of the tank (8.5 *cm* above the bottom of the tank), between the glass observation wall and the metal dividing wall. The steady air stream broke into bubbles that rose to create an upward buoyancy plume. Copper tubing carried the air from the laboratory compressor to the nozzle, by way of a pressure gage, as described in section 3.3. Air flow rate was controlled by the pressure gage (in kPa), which had been calibrated to flow rates in $\frac{mL}{s}$, as described in Appendix B.

Because the air nozzle was located near the bottom of the tank, special precautions were necessary to ensure that it would not become filled with water while the tank was being filled or left to acquire a linear stratification. The air tubing system was protected from water intrusion by means of a rubber hose placed securely over the exit nozzle before the tank was filled. This hose was directed up through the tank and out over one side, opening to the atmosphere. While the tank was being filled, the air was turned on to a moderately high flow rate (100 kPa), to keep water from

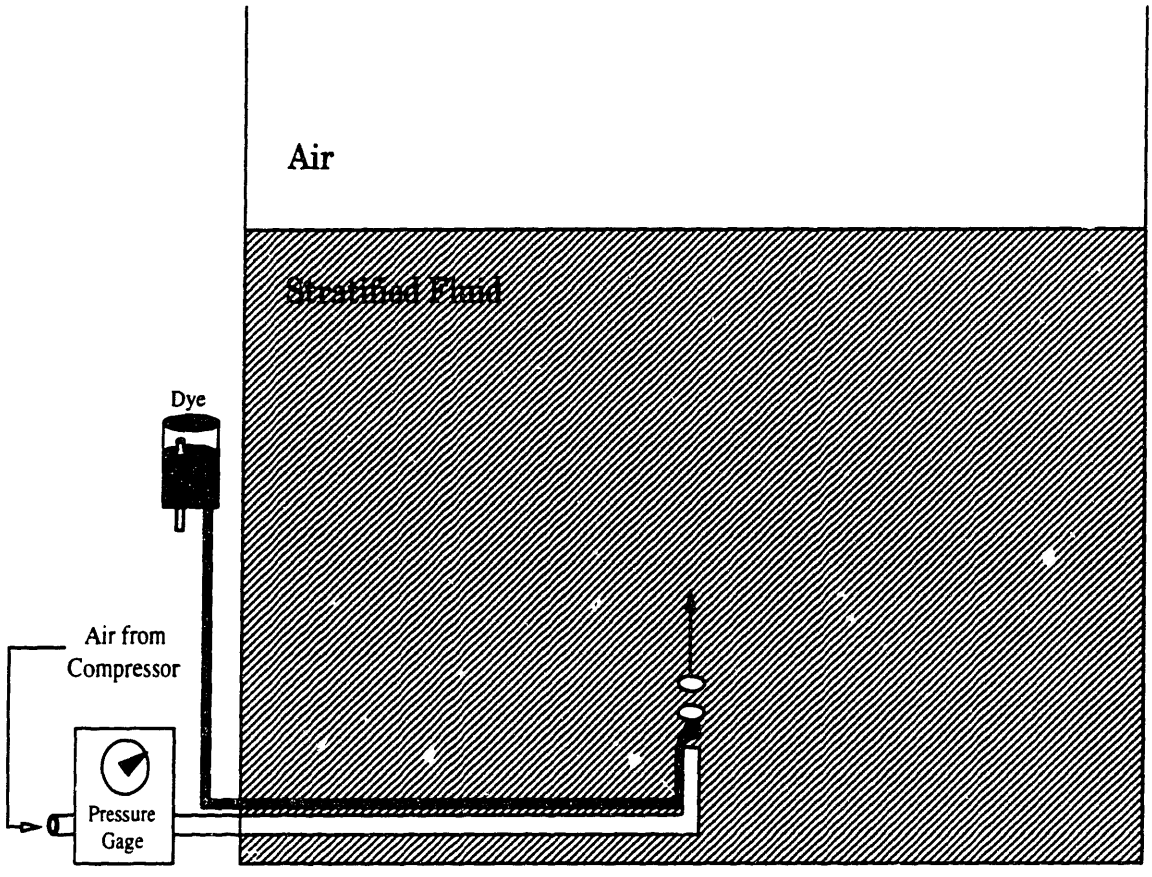

Figure 3-1: Bubble Plume Apparatus

leaking into the rubber hose, and to allow detection of hose leakage. Air bubbles never appeared around the rubber hose during filling, implying that the hose provided a secure seal with the air exit valve. The rubber hose remained over the air nozzle while the tank was reaching linear stratification; the air flow was discontinued once the tank had been filled.

At the start of each bubble plume experiment, before the rubber tube was removed, the air was again turned on, this time to the desired experiment flow rate. Air was allowed to run for five to ten minutes at the desired flow rate before the rubber hose was removed, to minimize start-up effects caused by pressure changes. When the air was flowing steadily through the rubber hose at the desired pressure, the pressure gage "hold" switch was enabled, to keep the air flow rate constant. Dye flow was then initiated, and the rubber tube was removed very gently (to minimize mixing). This began the observation period of the bubble plume.

Dye was injected as a passive tracer during each experiment, from a valve immediately abutting the air exit nozzle. The dye was introduced by means of a $\frac{1}{16}$ *in* plastic tube, connected to a bottle of darkly dyed liquid. This liquid was a solution of FD&C Blue No. 1 food coloring powder, dissolved in fluid extracted from the tank at air entry depth. The dye was thus of the same density as the ambient fluid immediately surrounding the air exit valve. Dye injection was begun shortly before bubbles were allowed to enter the tank, and continued throughout the experiment. Dye flow was regulated by an air entry valve in the dye source bottle. The bubble plume apparatus is depicted in figure 3-1.

Bubble plumes were allowed to run until the near-field profile had stabilized, but not long enough to create boundary effects from recirculation of dye at the edges of the tank. This time period was about four minutes. Observations were obtained visually and photographically, with the aid of a mounted tape measure and stopwatch. Record was kept of the plume peeling height over the course of the experiment; this was measured as the distance between the air nozzle and the center of the intrusion layer that formed as the plume progressed.

3.4.3 Sediment

Sediment plumes were created by the steady introduction of small sediment particles into the tank. Sediment was sifted to the correct diameter, as discussed in section 3.3. A plastic jug was suspended upside-down, with a pierced lid through which sediment of the appropriate diameter flowed at a measured flow rate. (The mass flow rate was determined by preliminary tests with a balance and stopwatch.) The jug was perforated on one side, to eliminate flow stoppage due to vacuum.

Sediment plumes were created by inverting the sediment jug at the water surface. The initial agitation of the jug as it was placed upside-down started the flow of sediment into the tank. The jug was mounted between the glass observation wall and the metal dividing wall, with its orifice at the water surface. The sediment plume began when sediment was allowed to exit the jug.

At the start of each sediment plume experiment, dye flow was initiated imme-

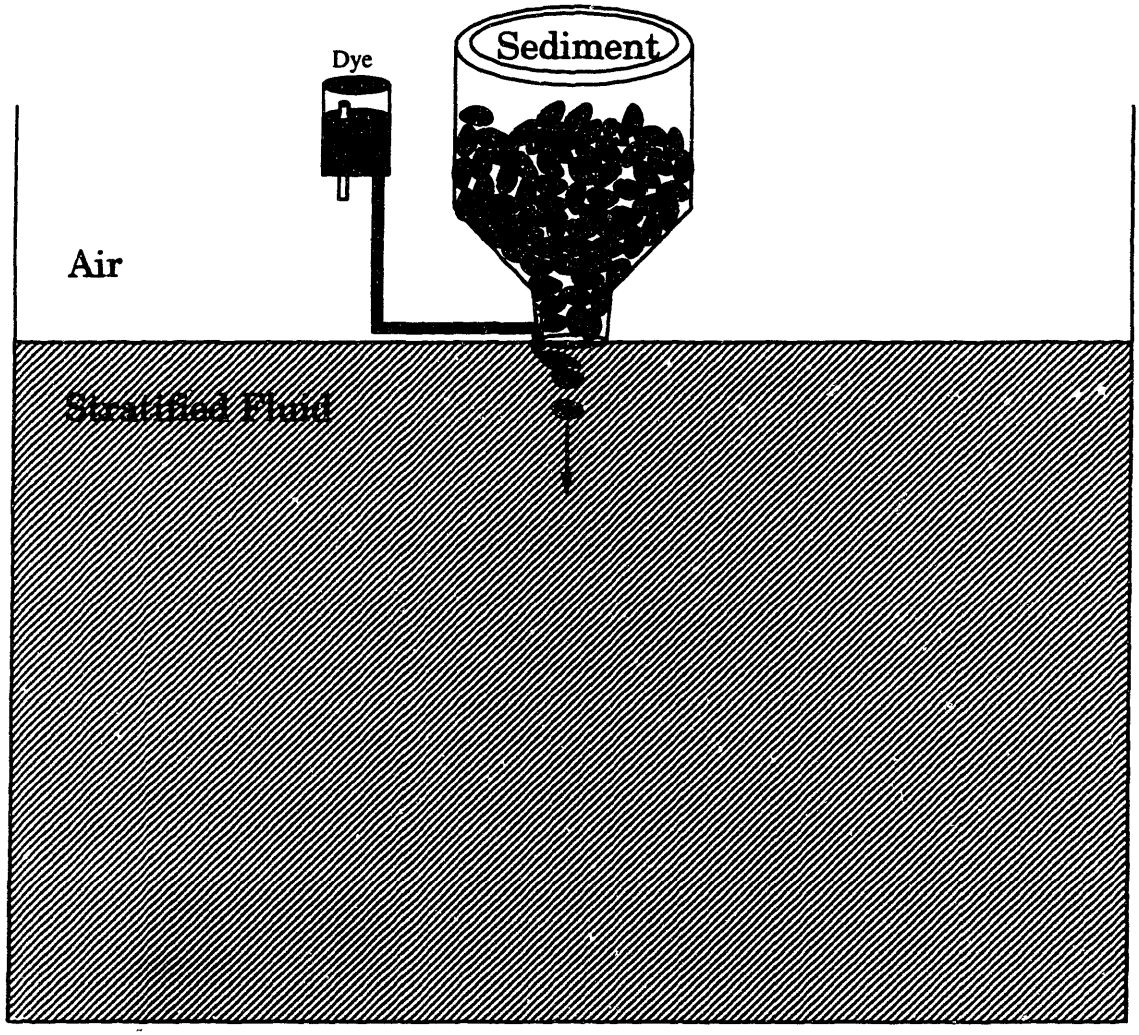

Figure 3-2: Sediment Plume Apparatus

diately before sediment flow. Dye was injected as a passive tracer during each run, from a valve immediately abutting the sediment exit orifice. As was the case with the bubble plume, a dye bottle with an air entry valve allowed the dye (which was of the same density as the ambient fluid immediately surrounding the sediment source) to flow through a plastic tube near the origin of the sediment plume. The dye injection was done in such a way as to create a precise parallel between the sediment plume tracing and the bubble plume tracing. The sediment plume apparatus is depicted in figure 3-2.

Sediment plumes were allowed to run for four to five minutes, similarly to the bubble plumes, until no further changes occurred in their near-field dye profiles, but not long enough for dye recirculation to begin at the edges of the tank. Observations were obtained visually and photographically, with the aid of a mounted tape measure and stopwatch. Record was kept of the plume peeling height over the course of the experiment. As with the bubble plumes, this height was the distance between the sediment source (at the top of the tank) and the center of the intrusion layer.

Chapter 4

Results and Conclusions

4.1 Results

Photographs of sample bubble and sediment plumes appear in figures 4-1, 4-2 and 4-3. Figure 4-2 shows the same plume as does figure 4-3, but figure 4-2 shows the plume at an earlier stage of development. The photograph in figure 4-1 was taken of a bubble plume that was recorded as an extra experiment for comparison with other models, and was not part of the set of experiments that were compared with sediment plumes. The plume parameters, however, were approximately the same as those in experiments 1 through 4. Figures 4-2 and 4-3 were taken during plume experiment 12.

AIR *Bubble Diameter = 0.7 cm*			
Experiment #	h_{exp}, *cm*	$N_h = \frac{B_0^{\frac{1}{4}}}{\varepsilon^{\frac{3}{8}}}$, *cm*	$\frac{h_{exp}}{N_h}$
1	22.5	13.4	1.68
2	22.5	13.4	1.68
3	22.5	13.4	1.68
4	22.5	13.4	1.68
AVERAGE	22.5	13.4	1.68

Table 4.1: Bubble Plume Data

Experiments	Q_0, $\frac{cm^3}{s}$	B_0, $\frac{cm^4}{s^3}$	*Salinity Range, ppt*	ε, $\frac{1}{s^2}$	v_t, $\frac{cm}{s}$
1, 2, 3, 4	3.6	3532	6.0 – 24.5	0.2300	19

Table 4.2: Bubble Plume Parameters

The bubble plume experiments produced very consistent data. The results of these experiments appear in table 4.1, where h_{exp} is the measured height from the air source to the peeling layer. N_h is a normalizing factor for the plume peeling height:

$$N_h = \frac{B_0^{\frac{1}{4}}}{\varepsilon^{\frac{3}{8}}}. \tag{4.1}$$

N_h is proportional to h_{max} (which is defined, along with B_0 and ε, in sections 2.3.1 and 2.3.2)—N_h is the same as h_{max} with no constant of proportionality. The density gradients were determined from tables [10], given the calibrated salinity measurements at the top and bottom of the tank in the experiments. The temperature of the tank was close to 25 ^0C during all of the plume experiments. Table 4.2 displays the experimental parameters for the bubble plumes.

Bubble plume peeling heights were within half a centimeter of each other for each trial, which was as close as could be measured with the instruments used. In every bubble plume experiment, the peeling layer occurred at 22.5 *cm* above the air orifice. Because all of the bubble trials show the same measured results, the uncertainty for these results is assumed to be due only to the limitations on the measurement techniques.

The first set of sediment plume experiments were performed on sediment meant to model the bubbles in the bubble plume trials, as described in section 3.2. Further ex-

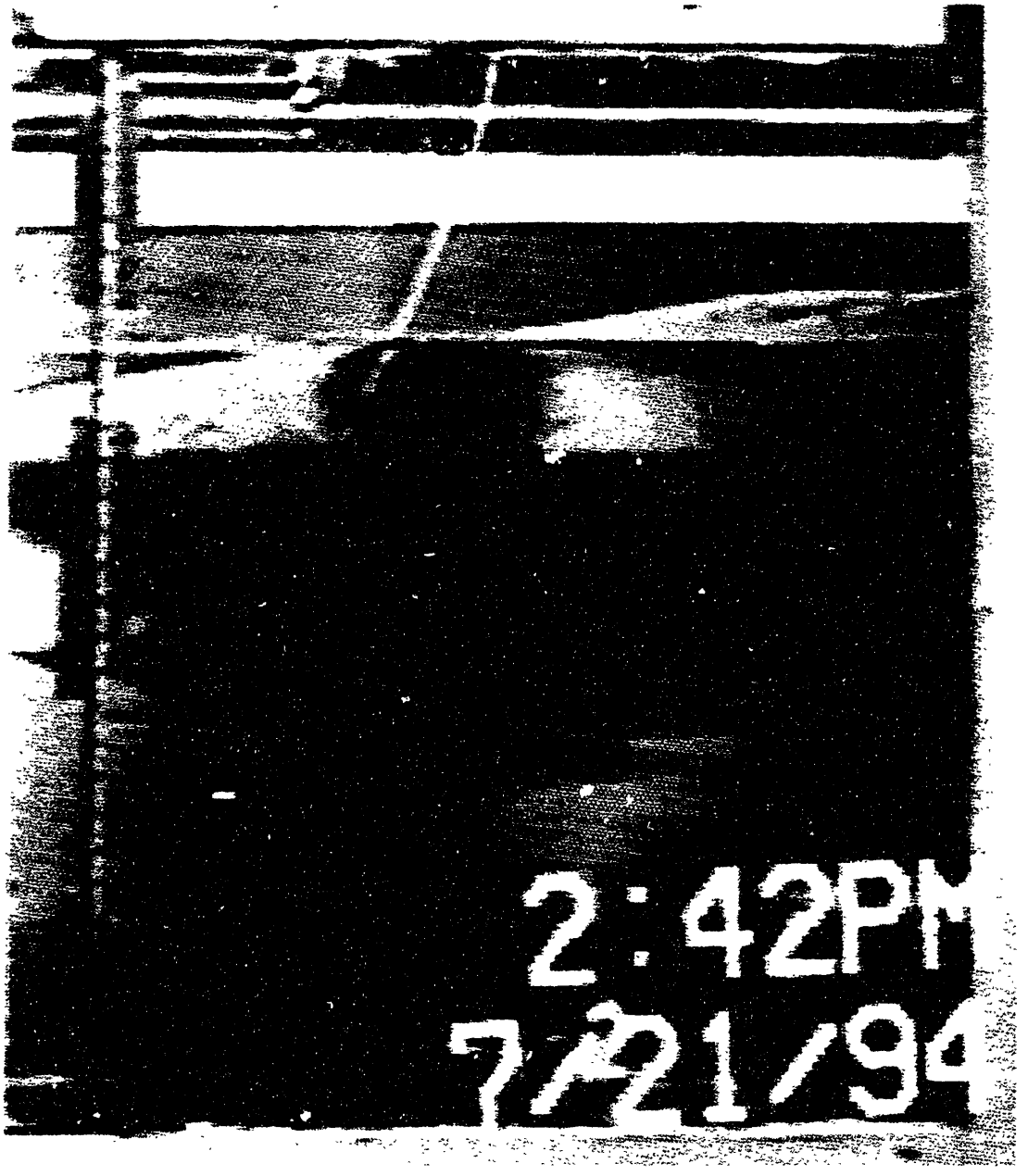

Figure 4-1: Photograph of a Sample Bubble Plume Experiment

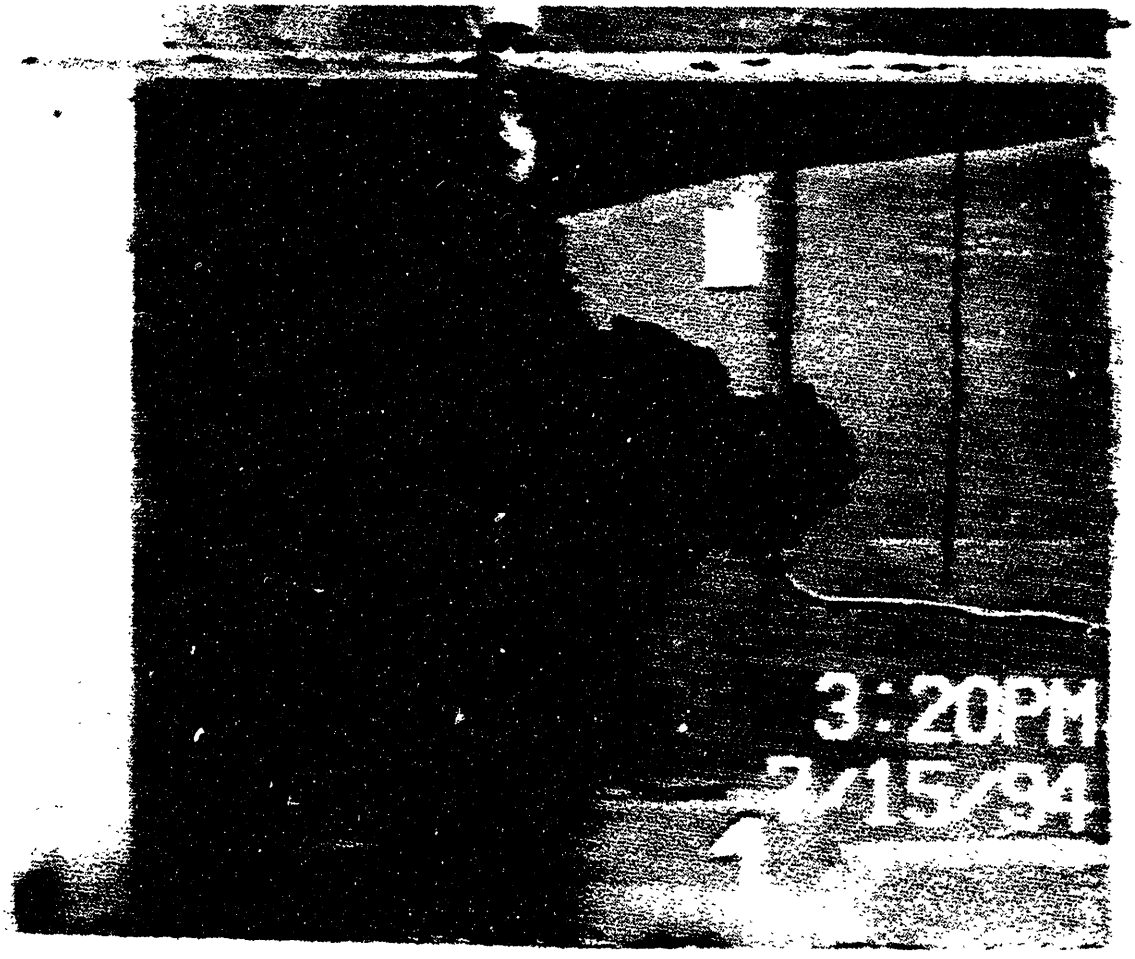

Figure 4-2: Photograph of Sediment Plume Experiment 12, Early Stage

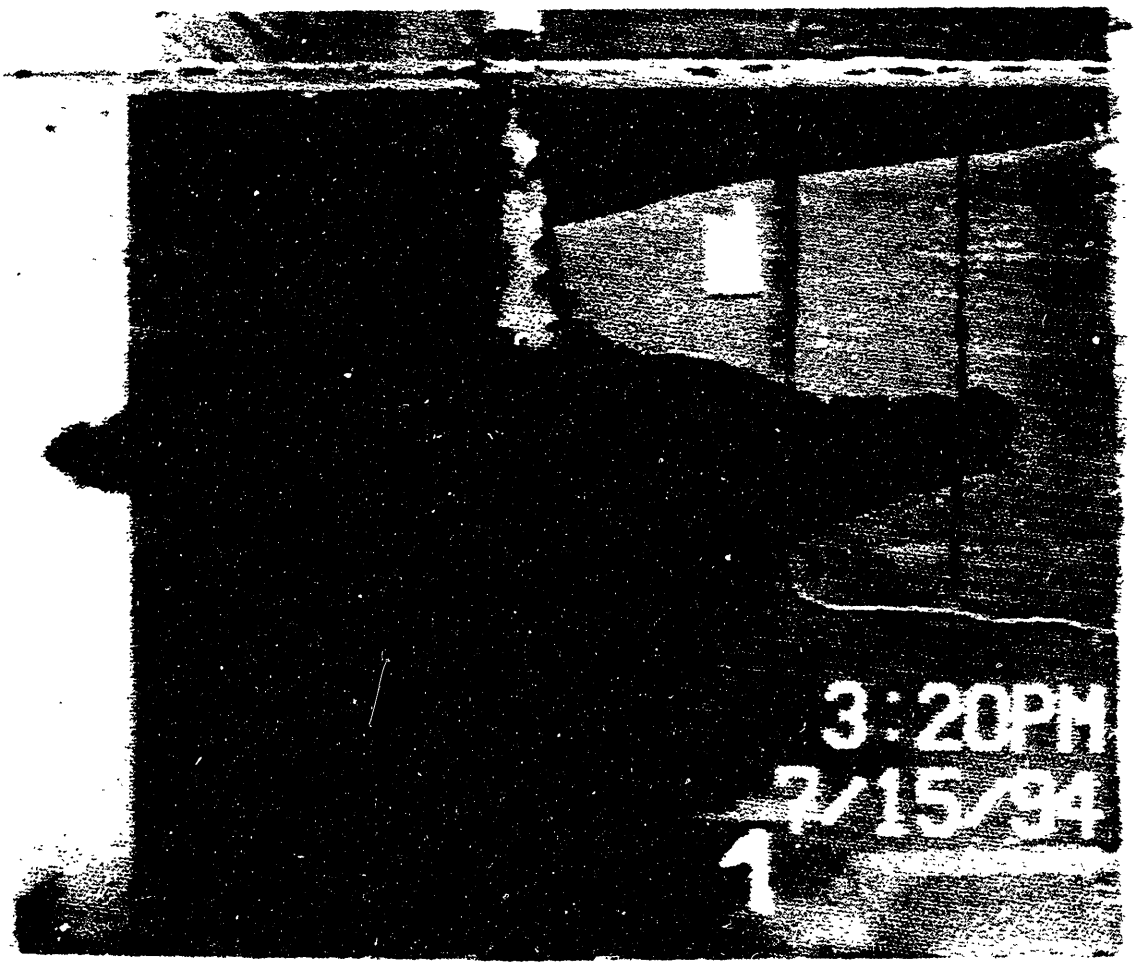

Figure 4-3: Photograph of Sediment Plume Experiment 12, Late Stage

SEDIMENT				
Experiment #	*Size Range*	h_{exp}, *cm*	$N_h = \frac{B_0^{\frac{1}{4}}}{\varepsilon^{\frac{3}{8}}}$, *cm*	$\frac{h_{exp}}{N_h}$
5	$1.41 - 2.83mm$	20.9	13.2	1.58
6	$1.41 - 2.83mm$	21.4	13.2	1.62
7	$1.41 - 2.83mm$	21.4	13.2	1.62
8	$1.41 - 2.83mm$	22.4	13.7	1.64
9	$1.41 - 2.83mm$	24.4	13.7	1.78
AVERAGE	$1.41 - 2.83mm$	22.1	13.4	1.65
10	$0.71 - 0.84mm$	24.0	11.9	2.02
11	$0.18 - 0.21mm$	22.5	9.32	2.41
12	$0.088 - 0.125mm$	22.9	8.68	2.64
and for comparison:				
13	*0 (Liquid)*	37.1	9.67	3.84

Table 4.3: Sediment Plume Data

Experiment(s)	$Q_0 = \frac{\dot{m}}{\rho_m}$, $\frac{cm^3}{s}$	B_0, $\frac{cm^4}{s^3}$	*Salinity Range, ppt*	ε, $\frac{1}{s^2}$	v_t, $\frac{cm}{s}$
5, 6, 7	2.25	3532	8.1 – 27.3	0.2404	19
8, 9	2.25	3532	6.7 – 24.5	0.2170	19
10	1.35	1989	6.5 – 23.4	0.2131	9.7
11	0.508	748	6.3 – 23.0	0.2143	2.1
12	0.430	633	6.3 – 24.6	0.2320	1.5
13	6.92	978	6.3 – 24.6	0.2320	—

Table 4.4: Sediment Plume Parameters

periments investigated smaller sediment in order to begin to analyze smaller bubbles, as mentioned in section 3.1. Another experiment was run with negatively buoyant fluid, as the lower limit on sediment size. The liquid in that plume had a density of 1.144 $\frac{g}{cm^3}$, and was released at the water surface from an inverted jug, following the sediment plume procedure described in section 3.4.3. The sediment and liquid data are shown in table 4.3, where h_{exp} is the measured depth between the surface sediment source and the peeling layer. The quantity N_h is defined exactly as it was for the bubble plumes; the salinity and density measurements were also determined in the same way, and the temperature in the tank was the same (around 25 ^0C). Table 4.4 shows the sediment plume experimental parameters.

Sediment plume trial results for the largest size range varied more than did bubble plume results; these experiments show more than 2 *cm* variation in peeling depth

measurements. The average peeling depth for these sediment trials, however, is assumed to be a good estimate of the plume behavior; this depth (22.1 *cm*) is within half a centimeter of the bubble plume peeling height.

4.2 Bubbles vs. Sediment, and Peeling Height Predictions

The data from the experiments indicate that peeling heights are the same (within measurement error) for positively and negatively buoyant plumes with the same buoyancy fluxes and terminal velocities relative to the ambient fluid. This result has several interesting implications, as discussed in section 2.2.

The calculation of $\frac{h_{exp}}{N_h}$ for the different sediment sizes allows the development of a graph for estimating peeling height based on diameter. The graph of that ratio (which is a normalized plume peeling distance) with respect to a representative diameter of the sediment is shown in figure 4-4. Each representative diameter is an arithmetic average of the endpoints of the relevant sediment size range. The error bar shown on one data point is also applicable to the other points on the graph; the other error bars are omitted to preserve clarity. With more data points from future experiments, this graph can be expanded and analyzed further. Because this graph shows normalized data, the resulting analysis can be applied to any plume, if the appropriate parameters are calculated and used.

Figure 4-5 displays the normalized peeling distance with respect to the terminal velocities of the sediment and bubbles. This plot allows a comparison of similar bubble and sediment plumes. Although most of the points on this curve are sediment data, the match of the existing bubble data to the sediment data at the same slip velocity is expected over the rest of the curve. The error bar on one of the points can be applied to any of the points on the graph; the other error bars are omitted for clarity.

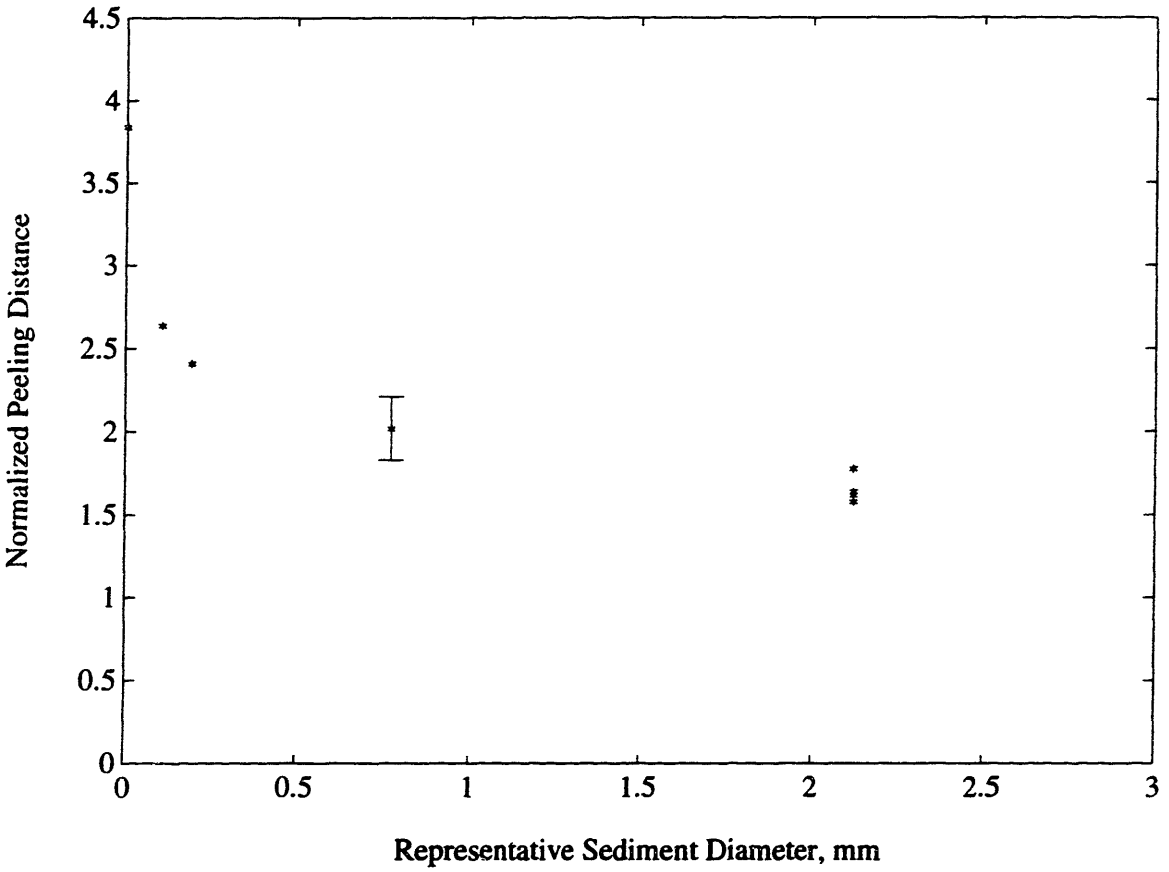

Figure 4-4: Normalized Peeling Distance vs. Representative Sediment Diameter

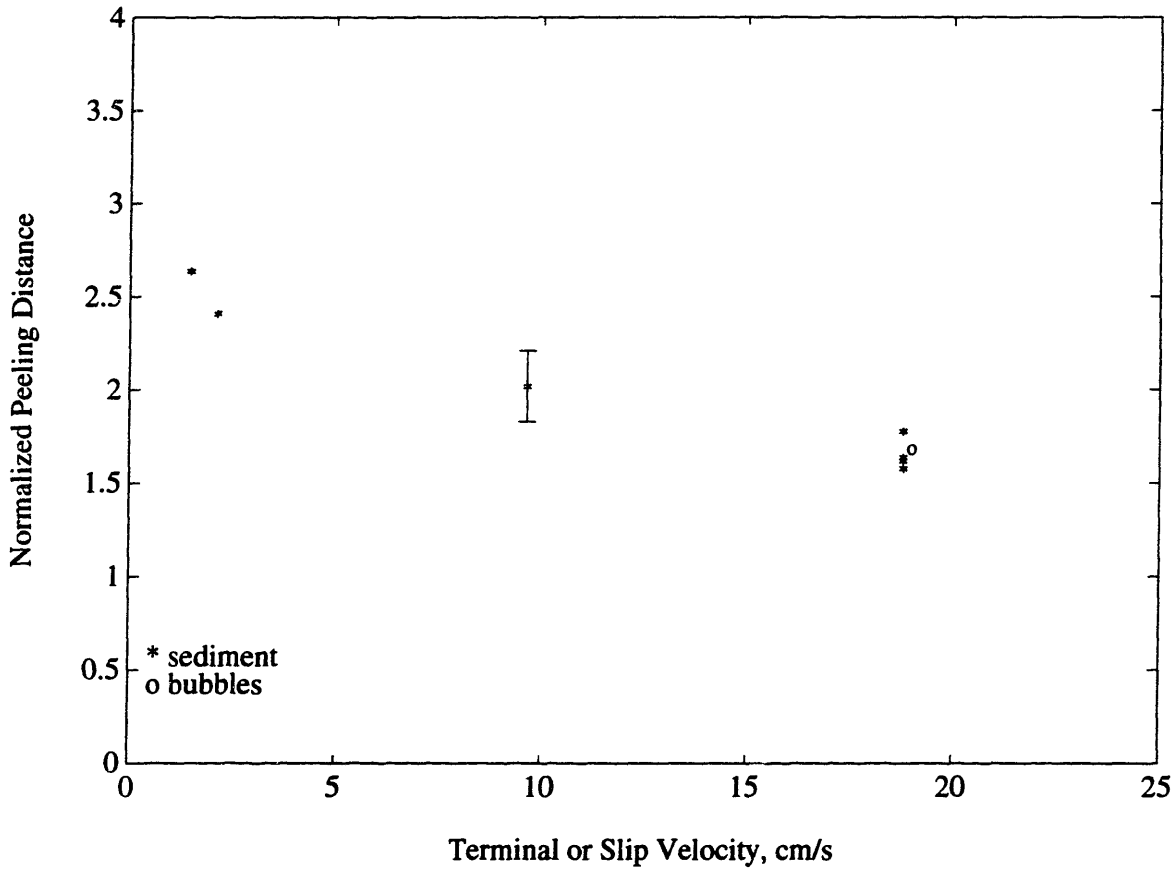

Figure 4-5: Normalized Peeling Distance vs. Particle Terminal Velocity

4.3 Error Analysis

4.3.1 Experimental Error

The experiments in this work were subject to inaccuracies in measurement and technique. These errors were then carried over into calculations during analysis. Each measurement of h_{exp}, the plume peeling height or depth, was subject to a visual observation error, estimated as 0.5 cm. For the average sediment peeling depth ($\bar{h_{exp}} = 22.1\ cm$), this is an error of 2.3%; for the average bubble peeling height ($\bar{h_{exp}} = 22.5\ cm$), it is an error of 2.2%. The bubble plume experiments were repeatable to within observation precision. The sediment experiments were repeatable to within $\sigma_{h_{sed}} = 2.3\ cm$, a variation of 10.4%

There is also room for error in calculations of B_0 and ε. B_0 was calculated (as discussed in section 2.3.2) from g (the gravitational constant), $\frac{\Delta\rho}{\rho}$ (the normalized density difference), and Q_0 (the sediment or bubble flow rate). ε was calculated (as discussed in section 2.3.2) from g, ρ (the ambient fluid density) and $\frac{d\rho}{dz}$ (the stratification gradient with depth). The errors in B_0 and ε were then compounded into error in $N_h = \frac{B_0^{\frac{1}{4}}}{\varepsilon^{\frac{3}{8}}}$. Estimates for errors in these parameters (based on measurement uncertainties) are shown in table 4.5.

A more detailed discussion of plume sensitivity to error in the tank density profile is provided in appendix C; that analysis indicates that an assumption of linear stratification is reasonable for the plumes in this work. The density gradient ($\frac{d\rho}{dz}$) is the greatest source of error for the plume parameters, but since ε, which relies on $\frac{d\rho}{dz}$, is raised to the $\frac{3}{8}$ power in N_h, the effect of the error is reduced.

4.3.2 Liquid as Limit of Sediment

The normalized peeling height of the liquid plume appears in figure 4-4 as a reference value, at zero representative diameter. Although this value would be expected to be the same as the normalized peeling height for the plumes of the smallest sediment (because these sediment grains were observed to be evenly distributed throughout

Parameter	*Estimated Measurement Error*
g	—
$\frac{\Delta\rho}{\rho}$	1%
Q_0	1%
$B_0 = g\frac{\Delta\rho}{\rho}Q_0$	2%
ρ	—
$\frac{d\rho}{dz}$	15%
$\varepsilon = \lvert\frac{g}{\rho}\frac{d\rho}{dz}\rvert$	15%
$N_h = \frac{B_0^{\frac{1}{4}}}{\varepsilon^{\frac{3}{8}}}$	5.1%

Table 4.5: Measurement Error in Basic Plume Parameters

the plume), the normalized peeling height for the liquid was larger than that for the smallest sediment size by a factor of around 1.5. This difference may be a result of a larger initial kinematic momentum flux in the liquid plume, making it resemble a jet more than did the sediment plumes. The initial kinematic momentum flux is:

$$M_0 = u_0 Q_0 = \frac{{Q_0}^2}{A_{orifice}}, \tag{4.2}$$

where u_0 is the initial average plume velocity, and $A_{orifice}$ is the plume orifice surface area. In the liquid plume, $M_0 = 380\ \frac{cm^4}{s^2}$; in the smallest sediment plume, $M_0 = 2.6\ \frac{cm^4}{s^2}$. These values differ by more than two orders of magnitude (by a factor of about 145). In a pure jet (single-phase), the reference maximum height of rise (analogous to h_{max} in section 2.3.2) is proportional to $\frac{M_0^{\frac{1}{4}}}{\varepsilon^{\frac{1}{4}}}$ [14]. In other words, treating both the liquid plume and the smallest sediment plume as though they were single-phase pure jets, the reference maximum rise heights would be expected to differ by a factor of $145^{\frac{1}{4}}$, or 3.5. Because neither plume was a pure jet, and in fact, the sediment plume was almost a pure plume, this factor of 3.5 is an over-estimate of the ratio of their maximum rise heights (assumed to be related to the ratio of the plumes' experimental peeling heights). Assuming, however, that the liquid plume was not a pure plume, and that it had some resemblance to a jet based on its high M_0, these calculations can account for the observed factor of 1.5 between the liquid and sediment peeling heights.

4.4 Liquid Plume Data vs. Single-Phase Theory

The negatively buoyant liquid plume was expected to behave according to the predictions in section 2.3.2 for single-phase buoyant plumes. Applying the formulas from section 2.3.2 to the experimental plume, $h_{max} = 36.7$, and h_{neut} was expected to be between 26.1 cm and 28.0 cm. The measured h_{exp} of 37.1 cm was just above the theoretical h_{max}, matching the single-phase theory within experimental error.

4.5 Bubble Plume Data vs. Previous Studies

McDougall (1978) performed bubble plume experiments, and Liro (1991) ran computer simulations of bubble plumes. Calculations were performed to compare the data for the bubble plumes in this work with the data obtained by both McDougall [25] and Liro [22].

In McDougall's bubble plume experiments [25], the bubbles were 1.25 mm in diameter; ε was 0.41 $\frac{1}{s^2}$, and Q_0 was 27 $\frac{cm^3}{s}$, leading to $B_0 = 2.65 \cdot 10^4$ $\frac{cm^4}{s^3}$. The McDougall N_h was therefore 17.8 cm. Since he observed peeling (h_{exp}) at 60 cm in his experiments, and at 45 cm in his computer simulation, his $\frac{h_{exp}}{N_h}$ (normalized peeling height) was 3.37 experimentally and 2.53 theoretically. According to McDougall, the bubbles in the plume had a slip velocity of 28 $\frac{cm}{s}$. The normalized peeling height values were higher than those obtained in this work for most of the smaller sizes of sediment, let alone the bubbles (which had even lower normalized peeling heights). The difference between McDougall's results and those in this work may be due to momentum effects, especially because McDougall was trying to maximize momentum effects in the plume, to approximate an oil-well blow-out problem.

For a sample Liro bubble plume simulation [22], $Q_0 = 0.831$ $\frac{m^3}{s}$, and the bubble plume was released at 500 m below the ocean surface. The density profile in the Liro model was used to calculate $\frac{d\rho}{dz} = 0.0021$ $\frac{kg}{m^4}$. These values led to $B_0 = 8.15$ $\frac{m^4}{s^3}$ and $\varepsilon = 2.1 \cdot 10^{-5}$ $\frac{1}{s^2}$, and thus $N_h = 95.9$ m. The bubble diameter was chosen to be 0.7 cm to match the bubbles in this work. The first peel in the Liro simulation

(which he assumed to be at the height of neutral buoyancy) occurred at 425.5 m below the surface, at 74.5 m above the plume source. The ratio $\frac{h_{exp}}{N_h}$ is then equal to 1.29 in Liro's theoretical analysis, which is about 77% of the value obtained in this work (1.68). The Liro result is smaller, which may be accounted for by the fact that the Liro model predicts peeling precisely at the height of neutral buoyancy of the plume, while the experimental bubble plumes in this work may have overshot that height before peeling, as discussed in section 2.3.2.

An auxiliary bubble plume experiment was performed as a rough comparison with the Liro peeling hypothesis [22] that half of the bubble plume volume flux is expected to flow away with each peel. Video recordings of the bubble plume allowed a rough estimate of the peeled volume flux (Q_{peeled}), and the total volume flux ($Q_{tot,plume}$) was estimated using a rearranged formula for single-phase buoyant plumes [27]:

$$Q_{tot,plume} = 0.155 B_0^{\frac{1}{3}} z^{\frac{5}{3}}. \tag{4.3}$$

The measured parameters were then $Q_{tot,plume} = 550\ \frac{cm^3}{s}$, and $Q_{peeled} = 170\ \frac{cm^3}{s}$. ($Q_{peeled}$ was calculated as the product of the average peeling-layer thickness, the front velocity of the peeling-layer and the breadth of the layer back into the tank, times a factor of two to include both sides.) These numbers lead to a calculated peeled volume fraction of about 30%, somewhat lower than Liro's assumption. Although the experimental result is approximate, the disparity between it and the Liro number indicates that the Liro assumption of the diverted fraction of volume flux may be an overestimate, at least for bubbles on the order of one centimeter in diameter.

4.6 Conclusions

The experimental results in this work indicate that sediment can be used as a model for bubbles to determine buoyant plume peeling heights. Peeling heights for all of the bubble and sediment plumes are smaller than the theoretical maximum heights of rise and heights of neutral buoyancy for single-phase plumes, as expected. The experi-

mental peeling height of the single-phase (liquid) plume is consistent with theoretical predictions. Sediment plume peeling heights increase with decreasing sediment size, but even at very small sediment diameters (as small as 0.088 mm, at which diameter the grains were evenly distributed throughout the plume), the peeling height does not approach that of a single-phase negatively buoyant plume. This may be because of greater momentum effects in the single-phase plume. Bubble plume peeling height data in this work is consistent with earlier studies; normalized peeling height in this work is lower than McDougall's theoretical and experimental values [25], but it is higher than Liro's theoretical values [22]. The estimated percent of a bubble plume's volume flux that peels to the sides is observed to be lower than predicted by Liro [22].

Appendix A

Stratification Lag Time

During stratification, the tank was filled with liquid in layers of distinct salinity, which were allowed to diffuse to a linear profile. Each layer was approximately 5.5 cm deep, and there were ten layers in the tank. Given the diffusivity coefficient of salt in water:

$$\varepsilon_{diff} = 1.35 \cdot 10^{-5} \frac{cm^2}{s}, \tag{A.1}$$

dimensional analysis reveals:

$$\varepsilon_{diff} \sim \frac{\mathcal{L}^2}{\mathcal{T}}, \tag{A.2}$$

so

$$\mathcal{T} \sim \frac{\mathcal{L}^2}{\varepsilon_{\text{diff}}} \tag{A.3}$$

where $\mathcal{L}$ is a characteristic path length of diffusion and $\mathcal{T}$ is a characteristic time of diffusion. As shown in figure A-1, diffusion occurs from the stepped profile (shown as a broken line) toward the straight line (shown as a solid line).

The solid line (linear profile) makes a series of triangles when superimposed on the broken line (initial profile). A characteristic path length of diffusion can be calculated as the distance between the solid line and an average distance travelled for the salt-water in the area contained by one triangle. The average distance of diffusion to the

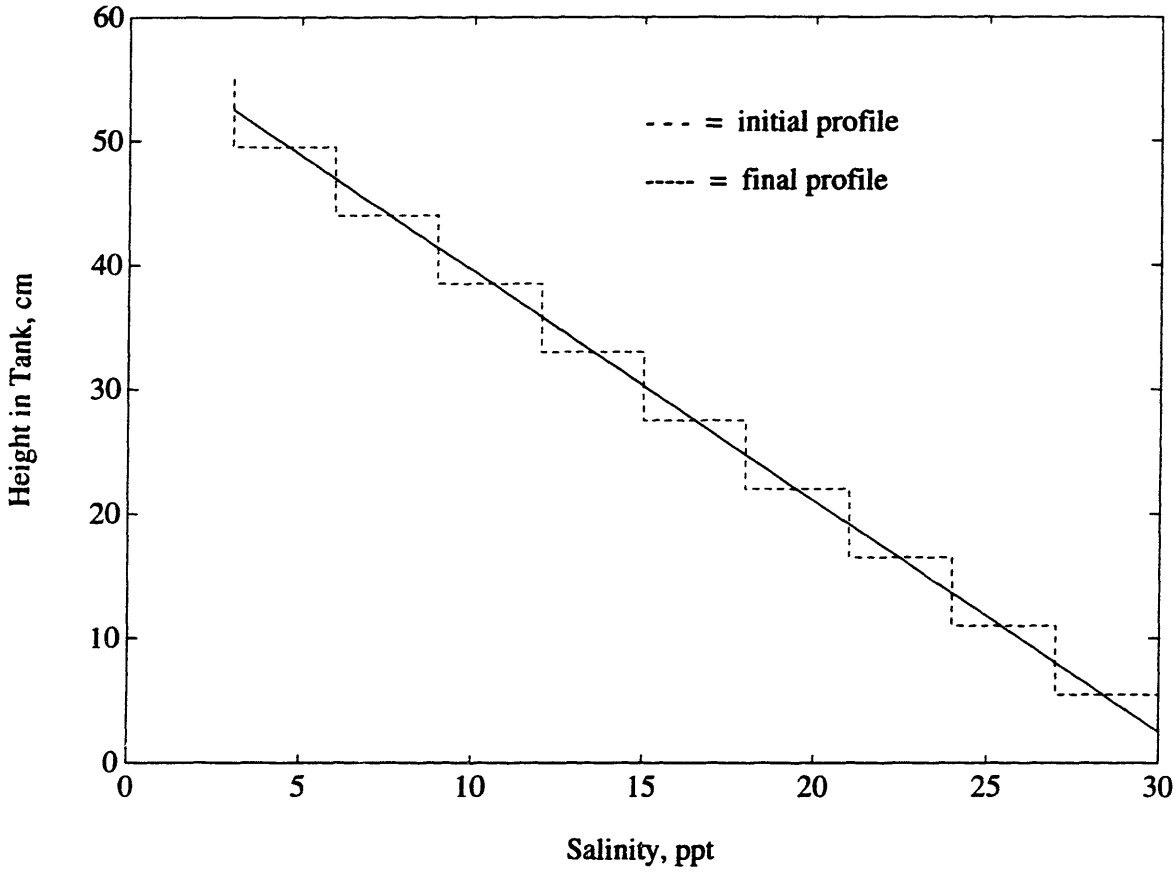

Figure A-1: Salinity Profile Before and After Becoming Linear

solid line is assumed to be an arithmetic average of the largest path of diffusion (the width of an entire layer) and the smallest path of diffusion (zero) in the triangle. This maximum diffusion path is then 2.75 cm, and so the mean characteristic path length of diffusion is:

$$\mathcal{L} = (\frac{1}{2}) \cdot (2.75cm + 0cm) = 1.38cm. \tag{A.4}$$

The characteristic time of diffusion is then:

$$\mathcal{T} = \frac{\mathcal{L}^2}{\varepsilon_{diff}} \tag{A.5}$$

$$\mathcal{T} = \frac{(1.38cm)^2}{1.35 \cdot 10^{-5} \frac{cm^2}{s}} \tag{A.6}$$

$$\mathcal{T} = 1.41 \cdot 10^5 s \tag{A.7}$$

$$\mathcal{T} = 39.2\text{hours} \tag{A.8}$$

This estimate does not include any mixing of the layers upon introduction to the tank, which is a conservative approximation. Before each plume experiment, the tank was left for 36 to 48 hours, and a salinity profile was measured immediately preceding each experiment. These profiles showed that the profile was indeed linear to within the precision of the salinity probe, which was calibrated with solutions of known salinity. A sample salinity profile is shown in figure A-2; this profile was measured at a temperature of 27.6 ^0C, for a bubble plume experiment.

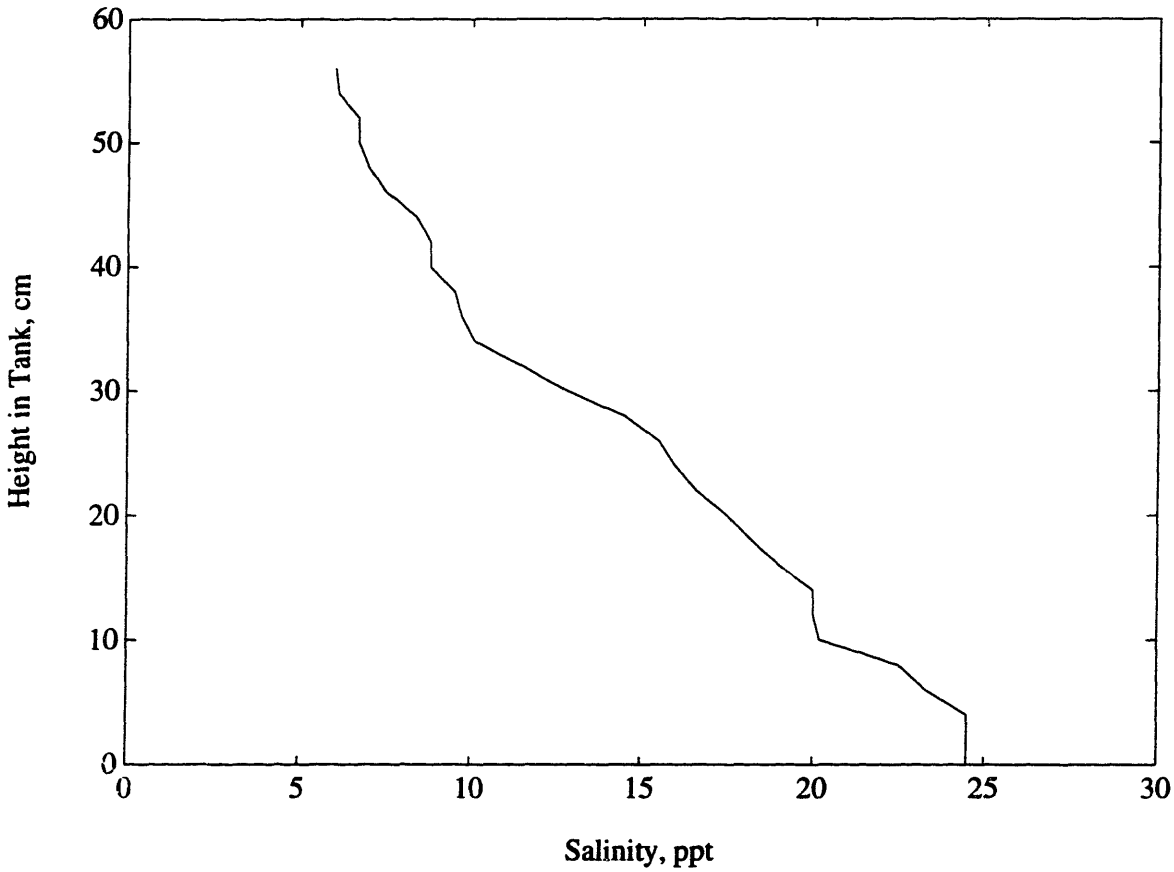

Figure A-2: Sample Salinity Profile, Measured at 27.6 Degrees Celsius

Appendix B

Air Flow Rate Calibration

To use the air pressure gage to monitor and control air flow rates, the gage (which measures air pressure in kPa) was calibrated to flow rate in $\frac{mL}{s}$. Air flow rate measurements were recorded for each of seven pressure settings. At each pressure setting, air flow rate was measured as the volume of water displaced by air in an overturned graduated cylinder that was filled with water and was then held over the air nozzle for a timed interval. Air was allowed to flow freely for five minutes before each volume measurement, to ensure that the pressure reading was not fluctuating on the gage, and that any residual water had been pumped out of the air pipe. Before measurements were taken, the "hold" switch was enabled to prevent fluctuations in air pressure.

The best fit plot of the flow rate data vs. the square root of pressure was a line, as shown in figure B-1. This line does not go through the origin, which may be due to a threshold pressure below which no air can exit the source. In any event, the experimentally determined line plotted regularly over an interval containing the desired range of air flow rates.

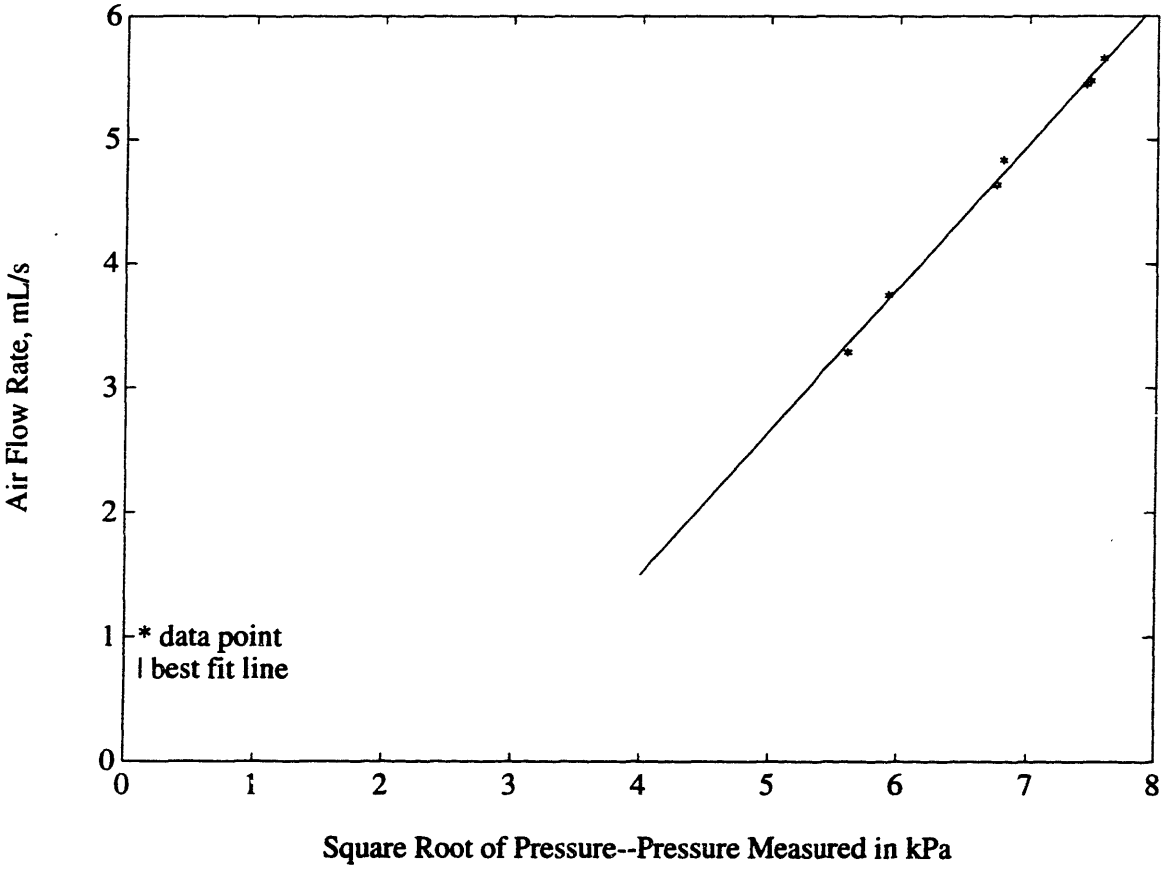

Figure B-1: Air Flow Rate vs. Square Root of Pressure

Appendix C

Plume Sensitivity to Stratification

The tank stratification was not perfectly linear, which may have had an effect on the normalization of the plume peeling height data. According to Brooks [7], calculations for plume reference heights can be modified in cases of non-linear density profiles. This is done by assuming a linear density profile over the portion of the tank through which the plume flows, neglecting the remaining salinity data. Because the sediment (and bubble) plumes flowed through the entire tank, this method was applied over the portion of the tank before the plume peeled.

The resulting re-calculation of $\frac{d\rho}{dz}$ for each case leads to new ε's, affecting the calculation of N_h. These calculations were performed on the sediment plume parameters, to investigate the sensitivity to stratification linearity of the plot of normalized peeling heights, figure 4-4. The modified values of ε appear in table C.1, along with the resulting $\frac{h_{exp}}{N_h}$ values and the old (non-modified) $\frac{h_{exp}}{N_h}$ values. The average value is shown for the $1.41 - 2.83\ mm$ diameter sediment.

As shown in table C.1, the modified data is very similar to the parameters de-

Experiment #	*Sediment Size Range*	$\varepsilon, \frac{1}{s^2}, (new)$	$\frac{h_{exp}}{N_h}, (new)$	$\frac{h_{exp}}{N_h}, (old)$
Average of 5 - 9	$1.41 - 2.83mm$	0.2099	1.60	1.65
10	$0.71 - 0.84mm$	0.2073	1.98	2.02
11	$0.18 - 0.21mm$	0.2240	2.45	2.41
12	$0.088 - 0.125mm$	0.1853	2.43	2.64

Table C.1: Modified Sediment Plume Parameters

termined under the assumption of a purely linear density stratification. The revised $\frac{h_{exp}}{N_h}$'s differ from those calculated under the assumption of linear stratification by as much as 10% at the smaller end of the sediment size range, but for the larger sediment sizes, the differences are smaller. The error of a few percent is not significant enough to prohibit an assumption of linear stratification.

There may also have been inaccurate salinity probe measurements, due to mixing during measurement. In an ordinary experiment, the salinity probe was raised slowly through the fluid, and the measured salinity was recorded every two centimeters, which may have caused inadvertent mixing. In order to estimate the error due to this extra mixing, the tank was stratified as usual, after which samples of liquid were extracted carefully from the top and bottom of the tank, and their salinities were measured.

The measured salinity of the liquid extracted from the top of the tank was 9.3 *ppt*; the measured salinity of the liquid extracted from the bottom was 19.5 *ppt*. The same profile, measured according to standard procedure with the salinity probe in the tank, measured a top salinity of 9.8 *ppt*, and a bottom salinity of 21.0 *ppt*. The bottom salinity was probably more accurate when measured directly in the tank, because the extraction tube may have had some fluid in it from the upper layers of the tank (explaining the lower measured salinity). (This is because the extraction tube was left in the tank during stratification, and although it was flushed with bottom-layer fluid before extraction, some residual upper-layer fluid may have remained inside.)

The top salinity was probably more accurate when measured from the extracted sample, because there was no apparent source of error in the technique, and because the slightly higher salinity measured in the tank indicates possible mixing during measurement. The two top salinity measurements are very similar to each other, however; the error is 0.5 *ppt* out of 9.3 *ppt*, or 5.4%. A 5% error in salinity measurement due to probe technique, in addition to the assumed error in measurement (in section 4.3.1) of 15%, would lead to a net N_h error of 7%, two percent more than the earlier estimate. This additional error is small enough that the original salinity measurements can be relied upon for the calculations in this work.

Appendix D

Parameters and Units Used

Parameter Name	*Description*	*Basic Units*
$A_{orifice}$	*Cross-Sectional Area of Plume Orifice*	$\mathcal{L}^2$
B_0	*Kinematic Buoyancy Flux*	$\frac{\mathcal{L}^4}{T^3}$
ε	*Square of Equivalent Stratification Frequency*	$\frac{1}{T^2}$
ε_{diff}	*Diffusivity Coefficient of Salt in Water*	$\frac{\mathcal{L}^2}{T}$
g	*Gravitational Acceleration*	$\frac{\mathcal{L}}{T^2}$
h_{exp}	*Measured Plume Peeling Height*	$\mathcal{L}$
h_{neut}	*Plume Height of Neutral Buoyancy*	$\mathcal{L}$
h_{max}	*Plume Maximum Rise Height*	$\mathcal{L}$
$\dot{m}$	*Initial Plume Mass Flow Rate*	$\frac{\mathcal{M}}{T}$
M_0	*Initial Plume Momentum Flux*	$\frac{\mathcal{L}^4}{T^2}$
N_h	*Peeling Height Normalization Factor*	$\mathcal{L}$
Q_0	*Initial Plume Volume Flow Rate*	$\frac{\mathcal{L}^3}{T}$
Q_{peeled}	*Volume Flow Rate of Peeled Plume Fraction*	$\frac{\mathcal{L}^3}{T}$
$Q_{tot,plume}$	*Plume Volume Flow Rate*	$\frac{\mathcal{L}^3}{T}$
ρ	*Ambient Fluid Density*	$\frac{\mathcal{M}}{\mathcal{L}^3}$
ρ_m	*Plume Material Density*	$\frac{\mathcal{M}}{\mathcal{L}^3}$
$\frac{d\rho}{dz}$	*Vertical Density Gradient*	$\frac{\mathcal{M}}{\mathcal{L}^4}$
$\frac{\Delta\rho}{\rho}$	*Normalized Density Difference*	—
$\sigma_{h_{sed}}$	*Variation in Sediment* h_{exp}	$\mathcal{L}$
u_0	*Initial Plume Average Velocity*	$\frac{\mathcal{L}}{T}$
v_t	*Sediment Terminal Velocity*	$\frac{\mathcal{L}}{T}$

Table D.1: Definition of Parameters

Symbol	*Definition*	*Quantity Measured*
cm	*centimeter*	*Length*
^0C	*degree Celsius*	*Temperature*
g	*gram*	*Mass*
in	*inch*	*Length*
kg	*kilogram*	*Mass*
kPa	*kiloPascal*	*Pressure*
m	*meter*	*Length*
mL	*milliliter*	*Volume*
mm	*millimeter*	*Length*
ppmv	*part per million, by volume*	*Concentration*
ppt	*part per thousand, by mass*	*Concentration*
s	*second*	*Time*

Table D.2: Unit Abbreviations

Bibliography

[1] Takasha Asaeda and Jörg Imberger. Structure of bubble plumes in linearly stratified environments. *Journal of Fluid Mechanics*, 249:35–57, 1993.

[2] ASCE. *Computer Simulation of Ice Control With Thermal-Bubble Plumes: Point Source Configuration*, Boston, MA, 1989.

[3] R. E. Baddour. Computer simulation of ice control with thermal-bubble plumes—line source configuration. *Canadian Journal of Civil Engineering*, 17:509–513, 1990.

[4] R. E. Baddour. Thermal-saline bubble plumes. *Recent Research Advances in the Fluid Mechanics of Jets and Plumes*, pages 117–129, 1994.

[5] W. D. Baines and A. M. Leitch. Destruction of stratification by bubble plume. *Journal of Hydraulic Engineering*, 118(4):559–577, April 1992.

[6] BHRA Fluid Engineering. *Size Distribution of Air Bubbles Entrained in Accelerated and Turbulent Water Flow*, September 1982.

[7] Norman H. Brooks. Dispersion in hydrologic and coastal environments. Technical report, California Institute of Technology, December 1972.

[8] Klas Cederwall and John D. Ditmars. Analysis of air-bubble plumes. Technical report, California Institute of Technology, 1970.

[9] R. Clift et al. *Bubbles, Drops, and Particles.* Harcourt Brace Jovanovich, Boston, 1978.

[10] The M. W. Kellogg Company. *Saline Water Conversion Engineering Data Book.* United States Department of the Interior, Piscataway, New Jersey, second edition, 1971.

[11] Todd V. Crawford and Arthur S. Leonard. Observations of buoyant plumes in calm stably stratified air. *Journal of Applied Meteorology*, page 254, June 1962.

[12] Julian A. Dowdeswell and Marianne Cromack. Behavior of a glacier-derived suspended sediment plume in a small arctic inlet. *Geological Notes*, 99:111–123, 1991.

[13] T. K. Fanneløp et al. Surface current and recirculating cells generated by bubble curtains and jets. *Journal of Fluid Mechanics*, 229:629–657, 1991.

[14] Hugo B. Fischer et al. *Mixing in Inland and Coastal Waters.* Academic Press, New York, 1979.

[15] Richard C. Flagan and John H. Seinfeld. *Fundamentals of Air Pollution Engineering.* Prentice Hall, Englewood Cliffs, New Jersey, 1988.

[16] International Hydrology and Water Resources Symposium. *Bubble Plumes and Mixing Efficiency in a Stratified Reservoir*, October 1991.

[17] ISEH. *A Design Methodology for Bubble Plume Destratification Systems*, December 1991.

[18] Warren T. Jones. Air barriers as oil-spill containment devices. *Society of Petroleum Engineers Journal*, pages 126–142, 1972.

[19] Albert Y. Kim and Donald F. Hayes. Model for turbidity plume induced by bucket dredge. *Journal of Waterway, Port, Coastal and Ocean Engineering*, 117:610–623, 1991.

[20] R. A. Kostaschuk et al. Suspended sediment concentration in a buoyant plume: Fraser river, canada. *Geo–Marine Letters*, 13:165–171, 1993.

[21] Charles J. Lemckert and Jörg Imberger. Energetic bubble plumes in arbitrary stratification. *Journal of Hydraulic Engineering*, 119(6):680–703, June 1993.

[22] Christopher R. Liro. Modelling the release of carbon dioxide in the deep ocean. Master's project, Massachusetts Institute of Technology, Department of Civil and Environmental Engineering, June 1991.

[23] Jay R. Lund. The decision to haul versus resuspend for hopper dredging. *Journal of Waterway, Port, Coastal and Ocean Engineering*, 117:599–609, 1991.

[24] Shiro Matesunashi. A field study on the characteristics of air bubble plume in a reservoir. *Journal of Hydroscience and Hydraulic Engineering*, 8(2):65–77, December 1990.

[25] Trevor J. McDougall. Bubble plumes in stratified environments. *Journal of Fluid Mechanics*, 85:655–672, 1978.

[26] J. H. Milgram. Mean flow in round bubble plumes. *Journal of Fluid Mechanics*, 133:345–376, 1983.

[27] W. P. Muellenhoff. Initial mixing characteristics of municipal ocean discharges. Technical report, U.S. Environmental Protection Agency, November 1985.

[28] Maynard Nichols et al. Effects of hopper dredging and sediment dispersion, chesapeake bay. *Environmental Geology Water Science*, 15(1):31–43, 1990.

[29] Robert E. Ricklefs. *Ecology*. W. H. Freeman, New York, third edition, 1990.

[30] D. M. Robertson et al. Interacting bubble plumes: The effect on aerator design. *Environmental Hydraulics*, pages 167–172, 1991.

[31] S. Geoffrey Schladow. Lake destratification by bubble-plume systems: Design methodology. *Journal of Hydraulic Engineering*, 119(3):350–368, March 1993.

[32] S. Geoffrey Schladow. Observations of artificial destratification. *Hydraulic Engineering '93*, page 957, 1993.

[33] John Wen and Robert S. Torrest. Aeration-induced circulation from line sources. i: Channel flows. *Journal of Environmental Engineering*, 113(1):82–98, February 1987.

[34] David L. Wilkinson. Two-dimensional bubble plumes. *Journal of the Hydraulics Division*, 105:139–154, February 1979.

[35] K. Zic et al. Laboratory study of water destratification by a bubble plume. *Journal of Hydraulic Research*, 30(1):7–27, 1992.